nature cell biology

ARTICLES

https://doi.org/10.1038/s41556-018-0261-6

AKT methylation by SETDB1 promotes AKT kinase activity and oncogenic functions

Jianping Guo[1,2], Xiangpeng Dai[2,3], Benoit Laurent[4], Nana Zheng[2], Wenjian Gan[2], Jian Zhang[5], Ailan Guo[6], Min Yuan[7], Pengda Liu[8], John M. Asara[7], Alex Toker[2], Yang Shi[4], Pier Paolo Pandolfi[9] and Wenyi Wei[2*]

Aberrant activation of AKT disturbs the proliferation, survival and metabolic homeostasis of various human cancers. Thus, it is critical to understand the upstream signalling pathways governing AKT activation. Here, we report that AKT undergoes SETDB1-mediated lysine methylation to promote its activation, which is antagonized by the Jumonji-family demethylase KDM4B. Notably, compared with wild-type mice, mice harbouring non-methylated mutant *Akt1* not only exhibited reduced body size but were also less prone to carcinogen-induced skin tumours, in part due to reduced AKT activation. Mechanistically, the interaction of phosphatidylinositol (3,4,5)-trisphosphate with AKT facilitates its interaction with SETDB1 for subsequent AKT methylation, which in turn sustains AKT phosphorylation. Pathologically, genetic alterations, including *SETDB1* amplification, aberrantly promote AKT methylation to facilitate its activation and oncogenic functions. Thus, AKT methylation is an important step, synergizing with PI3K signalling to control AKT activation. This suggests that targeting SETDB1 signalling could be a potential therapeutic strategy for combatting hyperactive AKT-driven cancers.

Epigenetic regulation, such as DNA methylation and histone modifications, plays important roles in governing gene expression patterns during human development and disease progression[1,2]. Inhibitors targeting epigenetic factors have been explored for cancer therapies and have undergone clinical trials, including DNA methyltransferase 1 inhibitors, histone deacetylase inhibitors and histone methyltransferase inhibitors[3–5]. Among these epigenetic inhibitors, those targeting histone methyltransferases (such as EZH2 and DOT1L) display impressive efficacy in patients with cancer[6,7]. This robust efficacy may also be attributed to the regulation of the methylation of non-histone proteins such as Rb and p53, in addition to regulating histone methylation[8–11]. However, it remains largely unknown whether predominant oncogenic signalling pathways that are frequently activated in human cancers, such as the PI3K–AKT signalling pathway, are subjected to methylation-dependent regulation. Thus, the identification of the major oncogenic proteins governed by methylation is critical to identify new therapeutic targets.

Hyperactivation of PI3K–AKT signalling is a central module of cell proliferation, survival and metabolic homeostasis in human cancers[12,13]. Physiologically, stimulations derived from various types of growth factors tend to activate AKT, which in turn phosphorylates distinct substrates to perform different biological processes[13,14]. Recently, emerging evidence has demonstrated that distinct signals govern AKT kinase activity. For example, the TRAF6- or SKP2-mediated positive regulation of AKT in a ubiquitination-dependent manner[15], the CDK2–cyclin A-mediated positive regulation of AKT in a tail phosphorylation-dependent manner[16] and the pVHL-mediated negative regulation of AKT in a hydroxylation-dependent manner[17]. However, the regulation of AKT by histone methyltransferases as a non-histone substrate is not well defined.

Here, we show that AKT1 methylation in its linker region is mediated by the histone methyltransferase SETDB1, which is antagonized by the demethylase KDM4B. Biologically, the absence of AKT1 methylation attenuates its kinase activity, which in turn represses cell growth, glucose uptake and tumorigenesis. As a result, deficiency in AKT methylation can physiologically decrease mouse body size and can protect mice from developing carcinogen-induced skin tumours. Thus, our data unravel a profound role for the SETDB1–KDM4B axis in manipulating AKT activity and highlight the histone methyltransferase SETDB1 as a potential target for combating hyperactive AKT-driven tumours.

Results

Methylation of AKT enhances its kinase activity. To identify important non-histone proteins that are regulated in a methylation-dependent manner, we used a specific pan-lysine trimethylation (Kme3) antibody and performed a mass spectrometry (MS)-based screening of cell lysates derived from ovarian cancer cells[10] (Fig. 1a; Supplementary Fig. 1a). Notably, an AKT1-derived peptide was identified, containing methylated modifications at two nearby evolutionarily conserved lysine residues (K140 and K142) in the AKT1 linker region (Fig. 1b; Supplementary Table 1). Furthermore, AKT1 methylation was validated using the Kme3-specific antibody in cells

[1]The First Affiliated Hospital, Sun Yat-sen University, Guangzhou, China. [2]Department of Pathology, Beth Israel Deaconess Medical Center, Harvard Medical School, Boston, MA, USA. [3]Institute of Translational Medicine, The First Hospital, Jilin University, Changchun, China. [4]Division of Newborn Medicine and Epigenetics Program, Department of Medicine, Boston Children's Hospital, Boston, MA, USA. [5]Key Laboratory of Systems Biology, Institute of Biochemistry and Cell Biology, Shanghai Institutes for Biological Sciences, Chinese Academy of Science, Shanghai, China. [6]Cell Signaling Technology Inc., Danvers, MA, USA. [7]Division of Signal Transduction, Department of Medicine, Beth Israel Deaconess Medical Center, Harvard Medical School, Boston, MA, USA. [8]Department of Biochemistry and Biophysics, Lineberger Comprehensive Cancer Center, The University of North Carolina at Chapel Hill, Chapel Hill, NC, USA. [9]Division of Genetics, Department of Medicine, Beth Israel Deaconess Medical Center, Harvard Medical School, Boston, MA, USA. *e-mail: wwei2@bidmc.harvard.edu

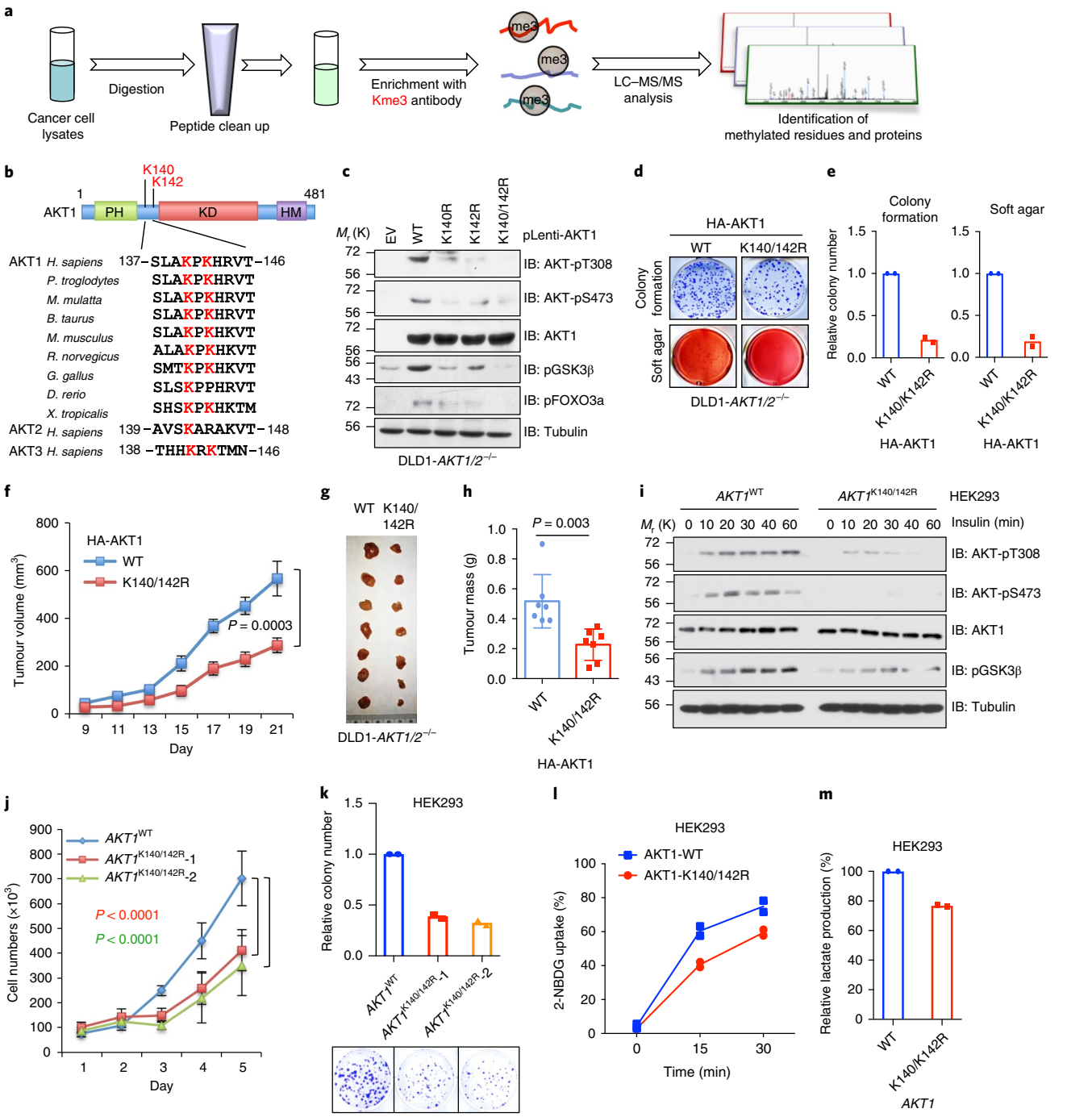

Fig. 1 | AKT methylation promotes its activity and oncogenic functions. a, A schematic workflow of IAP LC–MS/MS experiments. OVCAR5 cell lysates were proteolytically digested to perform IAP LC–MS/MS assays. **b**, Alignment of MS-characterized putative AKT1 methylation residues among different species, AKT2 and AKT3. PH, Pleckstrin homology domain; KD, kinase domain; HM, hydrophobic region. **c**, Immunoblot (IB) analysis of whole cell lysates (WCL) derived from DLD1-*AKT1/2*$^{-/-}$ cells infected with indicated *AKT1*-encoding lentivirus (Lenti) or empty lentivirus (EV) and selected with hygromycin (200 μg ml^{-1}) for 72 h before collection. Data shown represent two independent experiments. **d**,**e**, Cells generated in **c** were subjected to colony-formation and soft agar assays. The experiments were performed twice independently with three repeats, and exhibited similar results (**d**). Representative images are shown in **d**, and relative colony numbers derived from two independent experiments are plotted in **e**. **f**–**h**, Cells generated in **c** were subjected to mouse xenograft assays. Tumour sizes were monitored (**f**), and dissected tumours were weighed (**g**,**h**). Data in **f** and **h** represent the mean ± s.e.m., $n = 7$ mice. **i**,**j**, K140R and K142R mutations of *AKT1* were genetically engineered in HEK293 cells using the CRISPR–Cas9-based technique. Resulting cells were serum-starved for 12 h and then collected for IB analysis at different time points after stimulation with insulin (100 nM) (**i**). The experiment was performed twice independently with similar results (**i**). Cells generated in **i** were assessed for proliferation assays (**j**). The experiment in **j** was performed three times independently, and exhibited similar results. Data in **j** represent the mean ± s.e.m., $n = 3$ independent experiments. **k**–**m**, Cells generated in **i** were subjected to colony formation (**k**), glucose uptake (**l**) and lactate production (**m**) assays. The experiments were performed twice independently with three repeats, and exhibited similar results (**k**–**m**). Relative colony numbers, glucose and lactate levels derived from two independent experiments are plotted in **k**–**m**. Two-way ANOVA was performed in **f** and **j** to calculate the *P* values. Detailed statistical tests are described in the Methods. Source data for **e**, **f**, **h** and **j**–**m** are shown in Supplementary Table 2. Scanned images of unprocessed blots are shown in Supplementary Fig. 8.

treated with a global histone methylation inhibitor, 3-deazaneplanocin A (Supplementary Fig. 1b).

Additional MS analyses of ectopically expressed AKT1 further confirmed the trimethylation of K140 and K142, for which monomethylation and dimethylation events were also identified (Supplementary Fig. 1c). Moreover, K64, another lysine residue in the PH domain of AKT1, was identified to be monomethylated in our system. Interestingly, mutation of both K140 and K142 residues led to a dramatic reduction of AKT1 Kme3 signals in cells (Supplementary Fig. 1d), indicating that K140 and K142 might be the major AKT1 Kme3 residues. In addition, consistent with a previous report[18], deletion of *Smyd3*, a gene that encodes a methyltransferase targeting MAP3K2, did not disturb AKT kinase activity in cells, even though an interaction of SMYD3 with AKT1 has been previously reported[19] (Supplementary Fig. 1e–g). Given that both K140 and K142 sites were identified at endogenous levels through our large-scale non-biased MS approach, we chose to mainly focus on understanding the contribution of K140 and K142 trimethylation to AKT activity and oncogenic functions in the remainder of this study.

Absence of AKT methylation represses its oncogenic functions in cells and increases resistance to carcinogen-induced skin tumours in vivo. To reveal the potential biological functions of trimethylation within its linker region of AKT1, a methylation-deficient variant of AKT1 (K140R and/or K142R) was ectopically expressed in DLD1 cells in which both *AKT1* and *AKT2* were knocked out (DLD1-*AKT1/2*$^{-/-}$). Compared to wild-type AKT1 (AKT1-WT), the AKT1-K140/142R mutant, and to a lesser extent, AKT1-K140R and AKT-K142R, exhibited significantly reduced activation. This was shown by a marked reduction in AKT-pT308 and AKT-pS473, as well as its downstream targets, pGSK3β and pFOXO3a (Fig. 1c; Supplementary Fig. 1h–j). This observation was associated with a reduction in AKT1 kinase activity, as observed in vitro (Supplementary Fig. 1k). As a consequence, absence of methylation on K140 and K142 led to reduced cell colony formation, anchorage-independent growth, glucose uptake and lactate production in vitro (Fig. 1d,e; Supplementary Fig. 1l,m), and reduced tumour growth in vivo (Fig. 1f–h; Supplementary Fig. 1n,o).

To explore the role of AKT methylation under physiological conditions, we generated AKT1-K140/142R double mutations in HEK293 cells (termed *AKT1*$^{K140/142R}$) using CRISPR–Cas9 (clustered regularly interspaced short palindromic repeats–CRISPR-associated protein-9)[20] technology (Supplementary Fig. 1p–r). Notably, the presence of the K140/142R mutations in endogenous AKT1 decreased AKT phosphorylation in response to various stimuli (Fig. 1i; Supplementary Fig. 1s–u), and also compromised cell growth, colony formation, glucose uptake and lactate production (Fig. 1j–m). Next, we generated mice in which the AKT1-K140/142R double mutation was knocked in (termed *Akt1*$^{KI/KI}$) (Supplementary Fig. 2a–c). Compared with the WT mice, *Akt1*$^{KI/KI}$ mice exhibited a decrease in body size and weight (Fig. 2a,b; Supplementary Fig. 2d–f), organ size and weight (Fig. 2c; Supplementary Fig. 2g) and AKT kinase activity (Fig. 2d,e; Supplementary Fig. 2h), phenocopying *Akt1*$^{-/-}$ mice[21]. To pinpoint whether methylation-deficient mutants of *Akt1* abrogate tumorigenesis in vivo, we utilized a two-step chemical carcinogen (DMBA (7,12-dimethylbenzanthracene) followed by TPA (12-*O*-tetradecanoylphorbol-13-acetate))-induced skin tumour model[22]. In this model, we observed that *Akt1*$^{KI/KI}$ mice displayed a lower incidence of skin tumours and reduced papilloma burden compared with WT mice (Fig. 2f–h), which correlated with decreased AKT signalling (Fig. 2i). Together, these results support the notion that methylation of AKT in its linker region probably promotes AKT kinase activity and oncogenic functions both in vitro and in vivo.

SETDB1 methylates and activates AKT. Next, we set out to identify the physiological upstream methyltransferase (or methyltransferases) for AKT. Consistent with previous reports[23–25], we found that there was a relatively strong physical interaction between AKT1 and two trimethyltransferases, SETDB1 and EZH2 (Fig. 3a; Supplementary Fig. 2i). Interestingly, genetic alterations of both *SETDB1* and *EZH2* tended to mutually exclude alterations in PI3K–AKT pathway-related genes, including *PTEN* deficiencies, *EGFR*, *PIK3CA* or *AKT1* amplifications, or mutations in human melanoma and breast cancer[26] (Supplementary Fig. 2j). Furthermore, SETDB1, but not other methyltransferases, including EZH2, could enhance AKT trimethylation in cells (Supplementary Fig. 2i). This result indicates that unlike EZH2, which is a downstream substrate of AKT[25], SETDB1 may be an upstream regulator of AKT methylation (Supplementary Fig. 2k).

Notably, SETDB1 specifically interacted with the PH domain of AKT1 and, to a lesser extent, AKT2 and AKT3 (Fig. 3b; Supplementary Fig. 2l,m). Interestingly, mutation of AKT1 methylated residues (K140/142R) markedly decreased the interaction of AKT1 with SETDB1 (Supplementary Fig. 3a). Importantly, the Tudor domain of SETDB1 was identified to bind AKT1, which was enhanced by enforcing the expression of WT, but not the SETDB1-H1224K catalytic inactive mutant (Fig. 3c; Supplementary Fig. 3b). These results indicate that SETDB1 could be a potential reader of the AKT1-K140/K142 methylation events through its Tudor domain. Furthermore, by enhancing its interaction with AKT1, SETDB1 promoted AKT1 methylation on additional residues (such as K64). In addition, SETDB1 promoted AKT1 trimethylation in an enzymatic activity-dependent manner in cells (Fig. 3d), and mutation of the K140 and/or K142 residue decreased SETDB1-mediated AKT1 trimethylation in cells (Supplementary Fig. 3c). Moreover, ^{3}H-*S*-adenosyl-methionine (SAM)-mediated in vitro methylation assays also indicated that SETDB1 could directly methylate AKT1 at the K140 and K142 residues (Fig. 3e). Hence, these results coherently support the notion that SETDB1 serves as a putative AKT1 methyltransferase.

SETDB1 promotes cell growth and glycolysis through the methylation of AKT. As a histone H3 methyltransferase capable of catalysing trimethylation on K9 of histone H3 (H3K9me3)[27], SETDB1 is amplified in various cancers[28–31]. Notably, we identified that in addition to localizing in the nucleus and modifying histone marks, SETDB1 occurs in the cytoplasm of cells (Supplementary Fig. 3d). To further elucidate the physiological functions attributed to methylated AKT1, we generated specific antibodies against trimethylation of AKT1 at K140 (termed K140me3), which was validated by dot blot and immunoprecipitation assays (Supplementary Fig. 3e,f), and recognized SETDB1-mediated trimethylation of AKT1 at K140 in cells (Fig. 3f; Supplementary Fig. 3g) and in vitro (Fig. 3g; Supplementary Fig. 3h). Additionally, genetic depletion of *SETDB1* markedly reduced AKT1-K140me3 in cells (Fig. 3h–j; Supplementary Fig. 3i). Compared with AKT1-WT, a cancer patient-derived AKT1-E17K mutant[32] displayed an enhanced interaction with SETDB1, coupled with an increase in its K140 methylation level (Fig. 3k; Supplementary Fig. 3j,k). These findings suggest that AKT1 is a bona fide methylation substrate of SETDB1.

Importantly, genetic deletion of *Setdb1* in cells diminished AKT activation (Fig. 3i,j,l; Supplementary Fig. 3l–o). Furthermore, depletion of endogenous *SETDB1* by short hairpin RNA (shRNA) also reduced AKT-pT308 in different cancer cell lines (Supplementary Fig. 4a,b), leading to suppression of colony formation, anchorage-independent growth and glucose uptake in cells (Supplementary Fig. 4c–f). Conversely, ectopic expression of SETDB1-WT, but not SETDB1-H1224K[27], induced AKT-pT308 in *Setdb1*-deficient mouse embryonic fibroblasts (MEFs) (Fig. 3l). Collectively, these results indicate that the activation of AKT by SETDB1 appears to be methylation-dependent. Of note, consistent with a previous report[28], immunohistochemistry (IHC) staining revealed that compared to

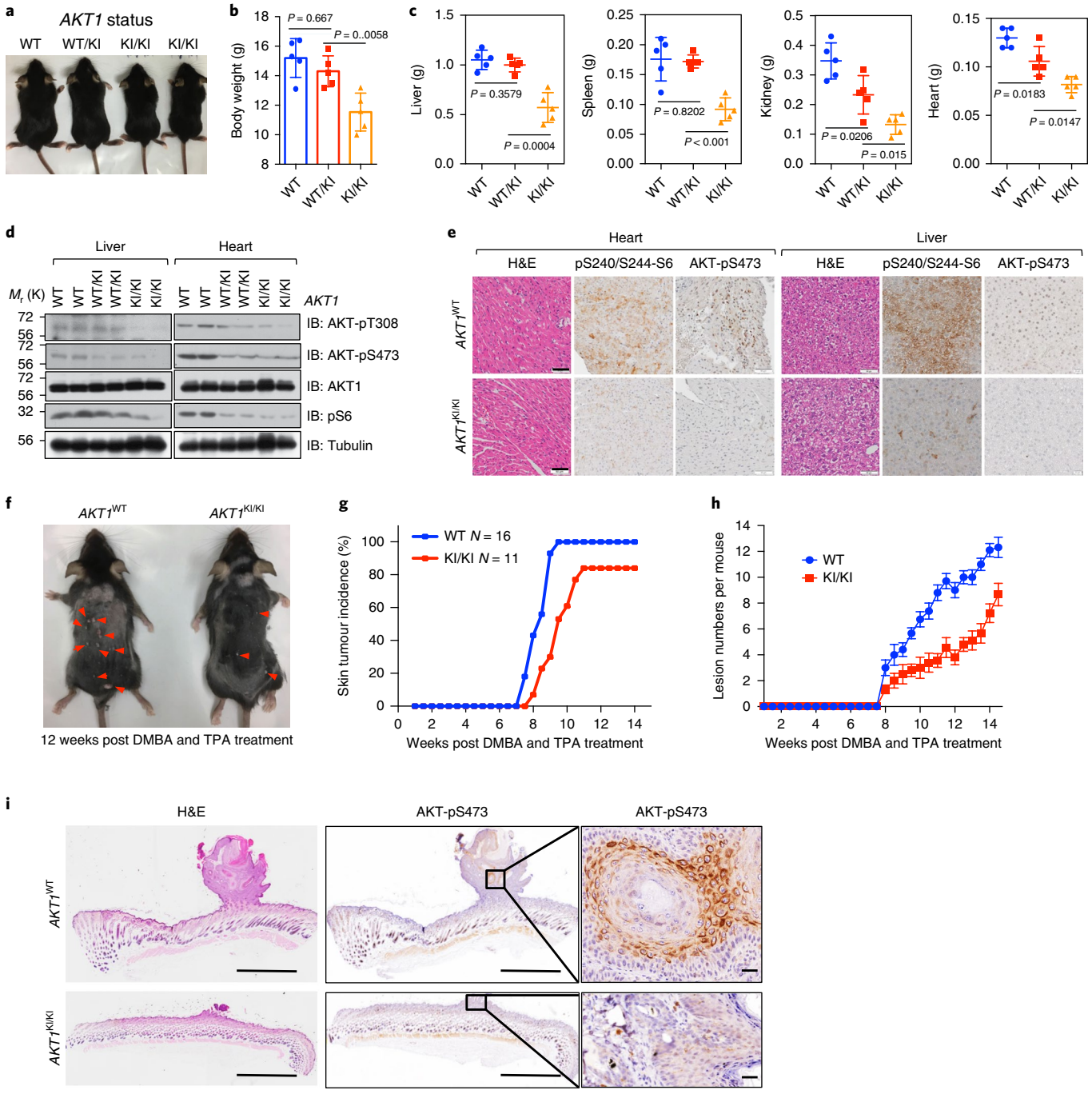

Fig. 2 | Methylation-deficient *Akt1* knock-in mice display reduced body size and weight and are resistant to chemical carcinogen-induced skin tumorigenesis in vivo. a, Mice derived from the same litter were imaged at 4 weeks of age. **b**, The 4-week-old mice were weighed (comprising 15 male mice, with 5 WT, 5 heterogeneous (WT/KI) and 5 homogenous *Akt1*$^{K140/142R}$ (KI/KI) genetic background status). Data represent the mean ± s.e.m., $n = 5$ mice. *P* values were calculated using two-tailed unpaired Student's *t*-test. **c**, The mice in **b** were killed and their organs were dissected and weighed. Data represent the mean ± s.e.m., $n = 5$ mice. *P* values were calculated using two-tailed unpaired Student's *t*-test. **d**, IB analysis of WCL derived from livers or hearts of WT, *Akt1*$^{K140/142R}$ knock-in heterogeneous or homogenous mice from the same litter at the age of 4 weeks. The experiment was performed twice, independently, with similar results obtained. **e**, Representative images of H&E and IHC staining of heart and liver tissues derived from WT or *Akt1*$^{K140/142R}$ knock-in mice. Scale bar, 50 μm. This experiment was performed twice independently, with similar results obtained. **f**, Side view of 12-week-old mice derived from WT or *Akt1*$^{K140/142R}$ knock-in mice treated with chemical carcinogen (DMBA followed by TPA). The neoplasm lesions are indicated by arrowheads. **g**,**h**, The tumour incidence (**g**) and lesion numbers (**h**) of the mice described in **f** were calculated and plotted. Data represent the mean ± s.e.m. ($n = 16$ mice for WT mice, $n = 11$ for *Akt1*$^{K140/142R}$ mice). **i**, After 12 weeks of treatment with DMBA and TPA, the mice were killed, and H&E (left) and IHC staining (right) were performed. Scale bar, 1 mm. The experiment in was performed twice independently, with similar results obtained. Statistical source data for **b**, **c**, **g** and **h** are shown in Supplementary Table 2. Scanned images of unprocessed blots are shown in Supplementary Fig. 8.

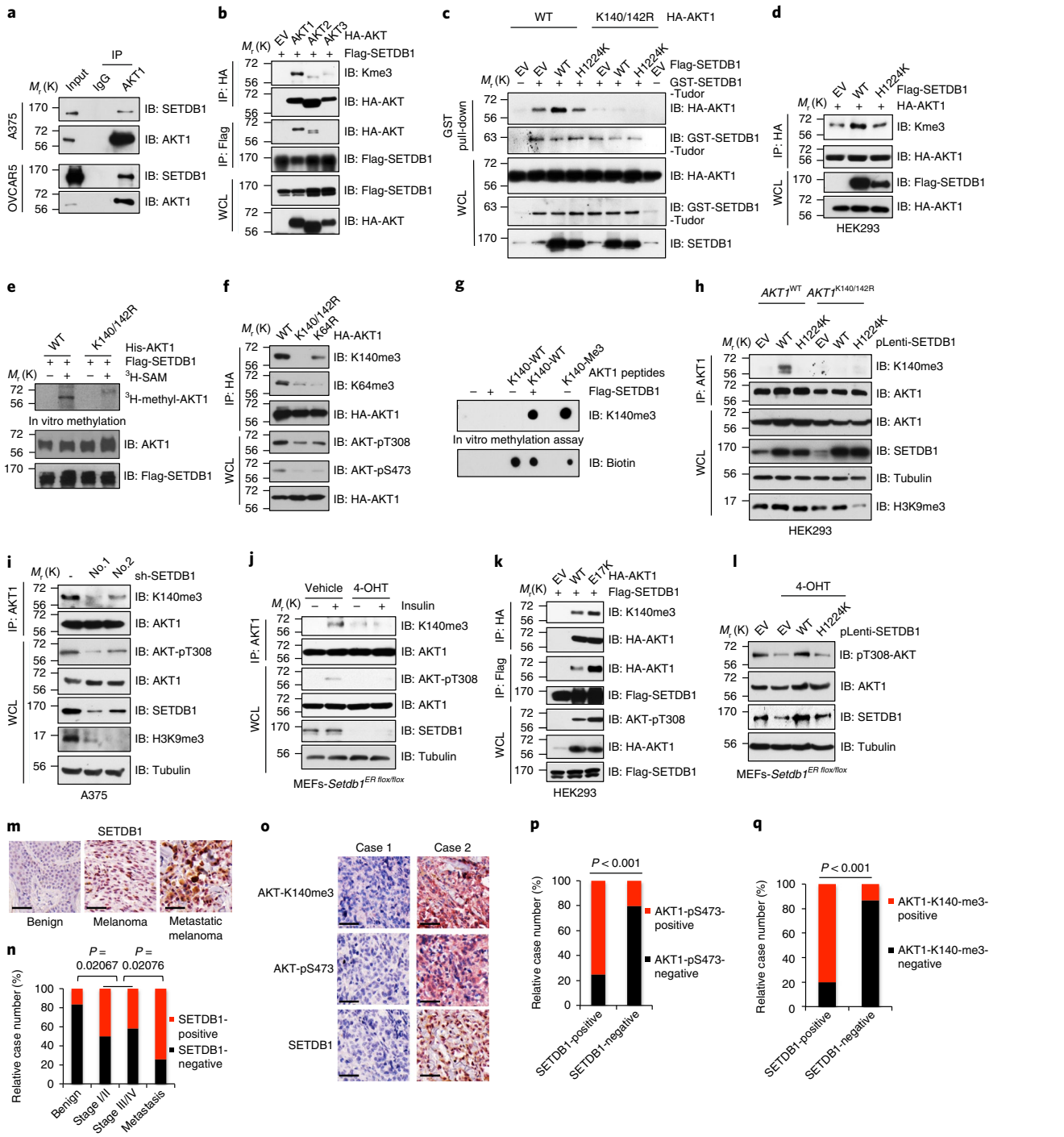

Fig. 3 | SETDB1 methylates AKT on K140 and K142 to promote its kinase activity. a–**d**,**f**,**h**, IB analyses of immunoprecipitation (IP) products, GST pull-down products and WCL derived from A375 and OVCAR5 (**a**) or HEK293 cells transfected with indicated constructs (**b**–**d**,**f**) or *AKT1*$^{K140/142R}$ knock-in cells stably expressing WT or catalytically inactive SETDB1-H1224K (**h**). IgG was used as a negative control. **e**, In vitro methylation assays were performed with recombinant His-AKT1 proteins purified from insect cells as substrates and purified Flag-SETDB1 from HEK293T cells as the source of methyltransferase in the presence or absence of ^{3}H-SAM. **g**, In vitro methylation assays were performed with IP Flag-SETDB1 derived from HEK293T cells as the source of methyltransferase, and the synthetic AKT1 peptides containing K140 and K142 as the substrates. AKT1-K140me3 peptides were used as a positive control. **i**, IB analyses of IP products and WCL derived from A375 cells lentivirally transfected with shRNAs against *SETDB1*. Resulting cells were selected with puromycin for 72 h before collection. **j**, *Setdb1* conditional knockout MEFs were treated with or without 4-OHT (4-hydroxytamoxifen, 500 nM) for 48 h to deplete endogenous *Setdb1*, then resulting cells were serum-starved for another 20 h and stimulated with insulin (100 nM) for 15 min before being collected and subjected to IP and IB analysis. **k**, IB analysis of IP products and WCL derived from HEK293 cells transfected with indicated constructs. **l**, *Setdb1* conditional knockout MEFs were infected with WT or H1224K-SETDB1 encoding virus and selected with puromycin for 72 h, then treated with or without 4-OHT (500 nM) for another 48 h before collection for IB analyses. **m**–**q**, Images of the IHC staining for SETDB1, AKT-pS473 and AKT-K140me3 in a melanoma tissue microarray (**m**,**o**). Scale bar, 50 μm. The distribution of SETDB1 staining is plotted in **n** ($n = 97$ tissue specimens). The correlation of AKT-pS473 or AKT-K140me3 with SETDB1 are plotted in **p** and **q** ($n = 95$ tissue specimens). Western blots in **a**–**l** were performed twice independently, with similar results obtained. *P* values were calculated using chi-squared tests in **n**–**q**. Statistical source data for **n**–**q** are shown in Supplementary Table 2. Scanned images of unprocessed blots are shown in Supplementary Fig. 8.

nevus tissues, SETDB1 is highly expressed in melanoma, especially in metastatic malignancies (Fig. 3m,n), and positively correlates with AKT1-K140me3 and AKT-pS473 IHC signals (Fig. 3o–q).

SETDB1 is suggested to accelerate melanoma onset in cooperation with $BRAF^{V600E}$ (ref. [28]). Given that coordinated actions of $BRAF^{V600E}$ with activated AKT are required to promote melanomagenesis[33,34], we employed a well-established human immortalized melanocyte (HIM) model[35] to examine whether SETDB1 modulates the activation of AKT. To this end, we found that concomitant activation of AKT and ERK signalling by SETDB1 and $BRAF^{V600E}$ led to a marked enhancement of anchorage-independent cell growth, coupled with increased AKT phosphorylation (Fig. 4a–c). Furthermore, deletion of endogenous *AKT1* in HEK293 cells compromised the oncogenic capability of SETDB1 to promote cell colony formation compared with parental cells (Fig. 4d–f).

More importantly, depletion of *SETDB1* resulted in decreased AKT phosphorylation and cellular malignant phenotypes in AKT1-WT-expressing DLD1-*AKT1/2*$^{-/-}$ cells, but did not in AKT1-K140/142R-expressing cells that already displayed relatively lower oncogenic capacity than WT cells (Fig. 4g–j). These results indicate that AKT is probably one of the major downstream pathways through which SETDB1 exerts its oncogenic role. Consistently, re-introduction of constitutively active AKT1 (myr-AKT1) partially restored the colony formation capability of *SETDB1*-depleted A375 cells (Supplementary Fig. 4g,h). Furthermore, SETDB1 was capable of accelerating cell growth and colony formation in $AKT1^{WT}$, but not in the methylation-deficient $AKT1^{K140/142R}$-expressing HEK293 cells (Fig. 4k–n). Hence, our results suggest that SETDB1 may exert its oncogenic roles largely through AKT activation in a methylation-dependent manner.

SETDB1-mediated AKT methylation crosstalks with PI3K-mediated AKT phosphorylation. It is well established that AKT activation requires the PI3K-dependent generation of phosphatidylinositol (3,4,5)-trisphosphate (PtdIIns(3,4,5)P_3), which binds to the PH motif of AKT at the plasma membrane[36–38]. We explored the temporal relationship between methylation-dependent and PI3K-dependent activation of AKT in cells. We found that the interaction between AKT1 and SETDB1, and subsequent methylation of AKT, temporally coincided with AKT-pT308 following insulin or insulin-like growth factor (IGF) stimulation (Fig. 5a; Supplementary Fig. 4i–k). Interestingly, PI3K inhibitors, but not AKT1 mutated variants (T308A and/or S473A), diminished the interaction of AKT1 with SETDB1 and decreased AKT1-K140 methylation in cells (Fig. 5b; Supplementary Fig. 4l,m). This indicates that the PI3K pathway may function upstream of SETDB1-mediated AKT methylation to govern AKT activation. In further support of this notion, the non-PtdIns(3,4,5)P_3 binding mutation of AKT1-R25C[39] largely impaired the interaction between AKT and SETDB1, leading to a marked decrease in AKT1-K140 methylation (Fig. 5c,d).

To further pinpoint the potential role of PtdIns(3,4,5)P_3 in mediating the interaction between SETDB1 and the PH motif of AKT1, we performed in vitro binding assays. The results showed that the interaction of SETDB1 with AKT1-WT, but not AKT1-R25C, was enhanced by PtdIns(3,4,5)P_3 in vitro (Fig. 5e; Supplementary Fig. 5a–e), indicating that PIP_3 binding could induce a conformation change in the PH motif, which facilitates AKT1 binding to SETDB1. Importantly, *PTEN* deficiency dramatically increased AKT1-K140 methylation coupled with increased AKT-pT308 (Supplementary Fig. 5f). Together, these data suggest that SETDB1 probably mediates AKT methylation in a PI3K catalytic activity-dependent manner.

Consistent with the finding that methylation of AKT1 could promote AKT-pT308, we observed that WT, but not the catalytically inactive SETDB1-H1224K, induced the interaction of AKT1 with PDK1 in cells (Fig. 5f; Supplementary Fig. 5g). Moreover, the methylation-deficient AKT1 mutant (K140/142R) or depletion of *SETDB1* displayed an attenuated interaction with PDK1 compared with AKT1-WT (Fig. 5g,h; Supplementary Fig. 5h). In further support of the role for AKT methylation in controlling its activation, reducing AKT methylation by deleting *Setdb1* or introducing the AKT1-K140/142R mutation diminished the interaction of AKT1 with PtdIns(3,4,5)P_3 (Fig. 5i,j), and subsequently led to a marked decrease in the association of AKT1 with the cell membrane (Fig. 5k,l; Supplementary Fig. 5i–m). These results indicate that methylated AKT1 may have a greater propensity to bind PtdIns(3,4,5)P_3 and translocate to the cellular membrane to achieve full activation. Thus, there is probably an intrinsic interplay between PI3K-mediated and SETDB1-mediated pathways to tightly control the spatial and temporal activation of AKT (Supplementary Fig. 5n).

Given that TRAF6-mediated AKT ubiquitination has a critical role in regulating AKT membrane translocation[15,40,41], we also found that WT, but not the SETDB1-H1224K mutant, increased the interaction between AKT1 and TRAF6 (Supplementary Fig. 5o), resulting in increased AKT ubiquitination (Supplementary Fig. 5p). Furthermore, compared with AKT1-WT, AKT1-K140/142R displayed a reduced interaction with TRAF6 (Supplementary Fig. 5q), resulting in decreased AKT ubiquitination (Supplementary Fig. 5r). These findings suggest that SETDB1-induced methylation probably mediates the interaction of AKT1 with TRAF6, and subsequent AKT ubiquitination may promote the membrane translocation of methylated AKT (Supplementary Fig. 5n).

KDM4B demethylates and attenuates AKT kinase activity. Importantly, the Jumonji 2 (JMJD2, also termed KDM4) family of proteins have been shown to function as specific erasers of SETDB1-mediated H3K9me3[42]; therefore, we assessed their ability to demethylate AKT1-K140me3. Notably, among all members of the KDM4 family, KDM4A and KDM4B, and to a lesser extent KDM4C, were observed to interact with AKT1 (Fig. 6a; Supplementary Fig. 6a). Furthermore, in vitro demethylation assays[42] demonstrated that KDM4B-WT, but not the catalytically inactive KDM4B-H189A or other KDM4 members, could efficiently erase the trimethylation of AKT1 at K140 in vitro (Fig. 6b; Supplementary Fig. 6b–e) and in cells (Supplementary Fig. 6f). Moreover, the interaction between KDM4B and AKT1 was readily induced by enforcing the expression of SETDB1-WT, but not its catalytic mutant (Fig. 6c). We further found that AKT1 interacts with KDM4B through its Tudor domain (Supplementary Fig. 6g–j) in a methylation-dependent manner (Fig. 6d,e; Supplementary Fig. 6k,l). Hence, these data indicate that KDM4B might be a bona fide demethylase of AKT1.

KDM4B depletion concomitantly increased AKT-pT308 and K140me3 in multiple cell lines with AKT1-WT, but not in $AKT1^{K140/142R}$ cells (Fig. 6f–h; Supplementary Fig. 6m–p). Strikingly, depletion of *KDM4A* led to a reduction in AKT phosphorylation levels (Supplementary Fig. 6q,r). In addition, depletion of *KDM4B*, but not *KDM4A*, largely enhanced AKT1 membrane translocation (Fig. 6i; Supplementary Fig. 6s). Furthermore, the interaction between AKT1 and KDM4B primarily occurred in the later phase of insulin stimulation (Supplementary Fig. 6t). This interaction was abolished by PI3K inhibitors (Fig. 6j). Consistent with the finding that KDM4B interacts with methylated AKT, the patient-derived mutation (AKT1-E17K) increased the interaction between AKT1 and KDM4B, while the non-PtdIns(3,4,5)P_3 binding mutation (AKT1-R25C) had the opposite effect (Fig. 6k). Clinically, KDM4B was expressed at relatively high levels in benign nevus compared to malignant melanoma (Fig. 6l,m). This observation correlated with decreased AKT-pS473 and K140me3 IHC signals (Fig. 6l,n,o). Taken together, these data suggest that KDM4B might function as a negative regulator, antagonizing SETDB1-mediated methylation and activation of AKT.

SETDB1 is a potential therapeutic target of AKT-driven cancers. Given the critical role for the PI3K–AKT pathway in facilitating

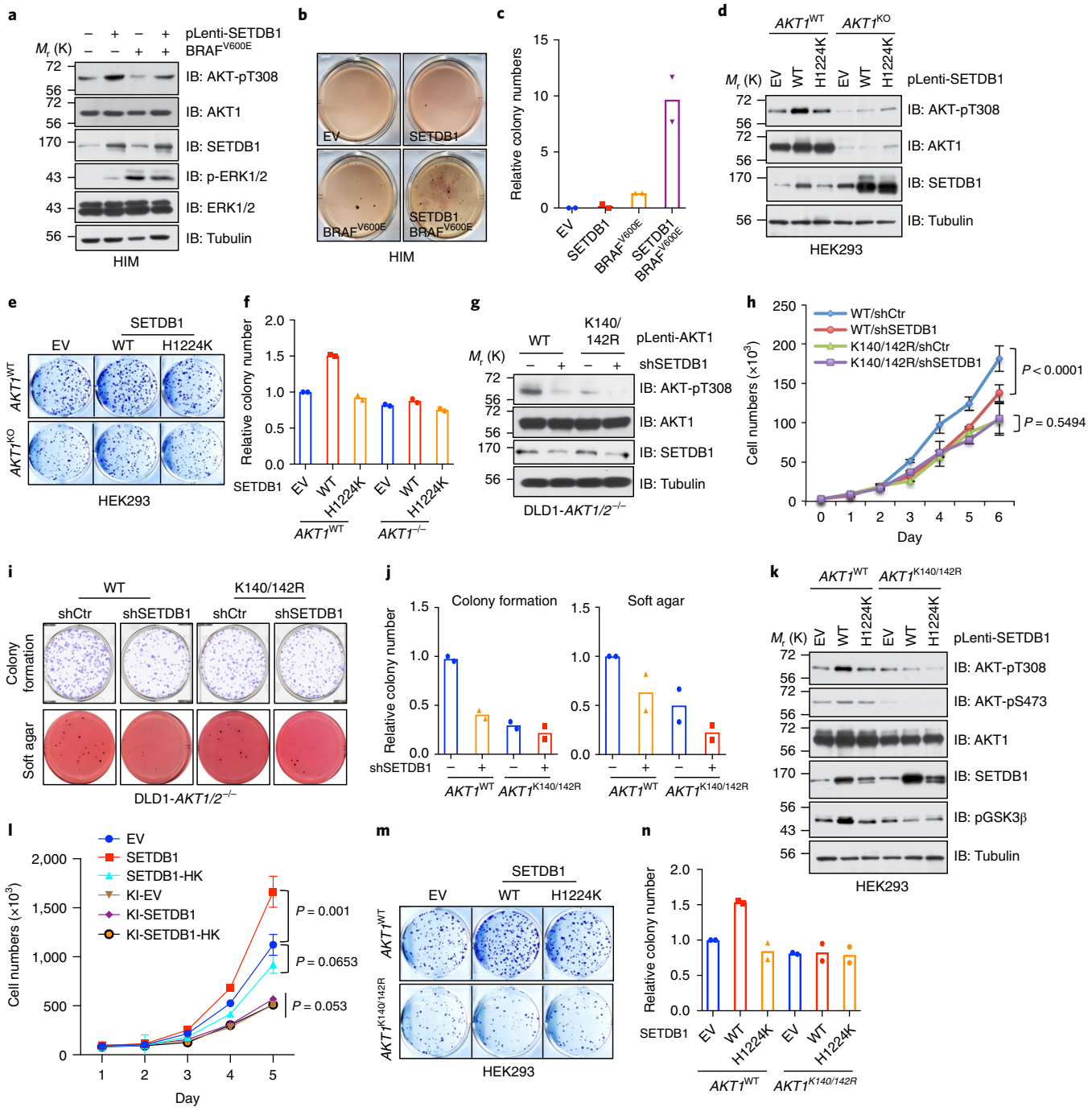

Fig. 4 | Oncogenic function of SETDB1 depends on the activation of AKT. a–c, HIM cells were lentivirally infected with indicated constructs, and selected with puromycin and hygromycin for 72 h before collection for IB analyses (**a**). Resulting cells were subjected to soft agar assays (**b**,**c**). **d**, IB analysis of CRISPR–Cas9-mediated *AKT1* knockout and parental HEK293 cells that were lentivirally infected with the constructs encoding SETDB1. **e**,**f**, Cells described in **d** were subjected to colony-formation assays. **g–j**, DLD1-*AKT1/2*$^{-/-}$ cells were infected with virus encoding WT or mutated AKT1, and selected with hygromycin for 72 h. Resulting cells were lentivirally infected with shRNA against *SETDB1* (with shCtr as a negative control) and selected with puromycin for 72 h. Cells were then collected for IB analysis (**g**), cell proliferation (**h**), colony-formation and soft agar (**i**,**j**) assays. **k–n**, *AKT1* $^{K140/142R}$-edited and parental HEK293 cells were lentivirally infected with SETDB1-WT or SETDB1-H1224K (SETDB1-HK) encoding constructs and selected with puromycin for 72 h before collection for IB analyses (**k**). Resulting cells were subjected to proliferation (**l**) and colony formation (**m**,**n**) assays. The experiments in **b**, **e**, **i** and **m** were performed twice independently with three repeats, and exhibited similar results. Relative colony numbers derived from two independent experiments are plotted in **c**, **f**, **j** and **n**. The cell proliferation assays in **h** and **l** were performed three times independently, and cell numbers were quantified in **h** and **l**. Data represent the mean ± s.e.m., $n = 3$ independent experiments. Two-way ANOVA was performed in **h** and **l** to calculate the *P* values. Detailed statistical tests are described in the Methods. Source data for **c**, **f**, **h**, **j**, **l** and **n** are shown in Supplementary Table 2. Western-blots in **a**, **g** and **k** were performed twice independently, with similar results obtained. Scanned images of unprocessed blots are shown in Supplementary Fig. 8.

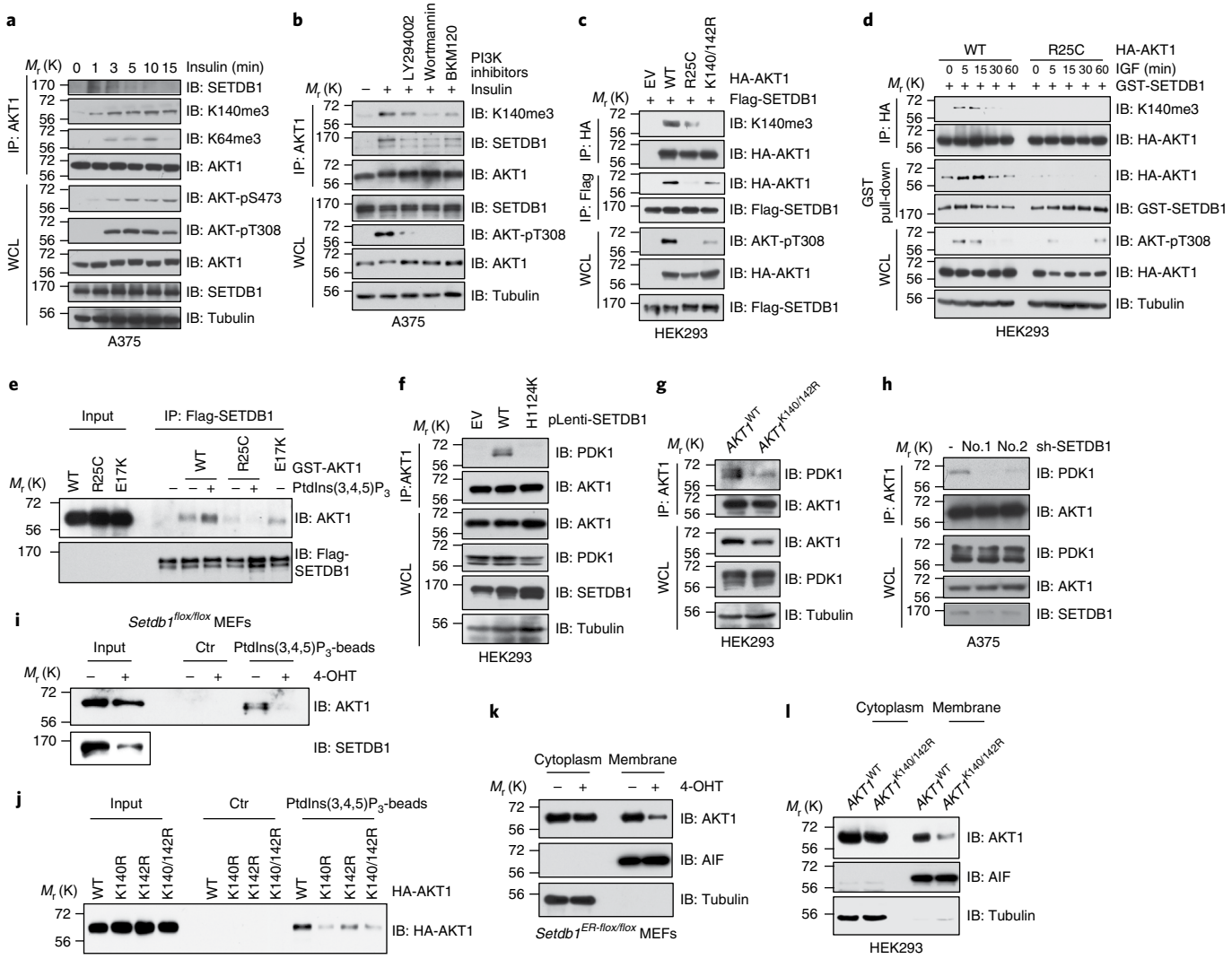

Fig. 5 | SETDB1-mediated methylation of AKT synergizes with PI3K to activate AKT. a,**b**, A375 cells were serum-starved for 20 h then stimulated with insulin (50 nM) at different time points (**a**) or post treatment with various PI3K inhibitors (**b**) before collection for IP and IB analyses. **c**,**d**, IB analysis of IP products and WCL derived from HEK293 cells transfected with indicated constructs stimulated without (**c**) or with IGF (100 ng ml^{-1}) (**d**) before collection. **e**, In vitro binding assays were performed with recombinant GST-AKT1 protein purified from mammalian cells, and Flag beads bound with SETDB1. The binding was performed at 4 °C for 4 h incubated with or without PtdIns(3,4,5)P_3 (20 μM) and subjected to IB analysis. **f**–**h**, IB analyses of AKT1 IP products and WCL derived from HEK293 cells infected with indicated SETDB1 encoding constructs (**f**), *AKT1*$^{K140/142R}$ and its parental HEK293 cells (**g**) and *SETDB1*-depleted A375 cells (**h**). **i**,**j**, IB analyses of PtdIns(3,4,5)P_3 pull-down products and WCL derived from *Setdb1* conditional knockout MEFs treated with or without 4-OHT (500 nM) for 48 h (**i**) or from HEK293 cells transfected with indicated constructs (**j**). Where indicated, empty beads (Ctr) serve as a negative control. **k**,**l**, IB analyses of cell fractionations separated from *Setdb1* conditional knockout MEFs treated with or without 4-OHT (500 nM) for 48 h (**k**) or from *AKT1*$^{K140/142R}$-edited and parental HEK293 cells (**l**). All western blots were performed twice independently, with similar results obtained. Scanned images of unprocessed blots are shown in Supplementary Fig. 8.

tumorigenesis, targeting hyperactive PI3K–AKT signalling via PI3K and/or AKT inhibitors has been pursued as a promising anticancer therapeutic approach. However, relatively high doses of these inhibitors induces cellular toxicity, restricting their potential use as a treatment option in patients with cancer[43,44]. Thus, our finding that SETDB1 synergizes with PI3K to activate AKT kinase (Supplementary Fig. 7a) indicates that SETDB1-specific inhibitors could benefit patients with cancer by targeting both H3K9-mediated epigenetic and PI3K–AKT oncogenic pathways. In support of this hypothesis, we found that depletion of *SETDB1* significantly decreased A375 tumour growth in vivo (Fig. 7a–d), which was coupled with a reduction in H3K9me3 and AKT phosphorylation (Fig. 7e).

Consistent with a previous report[45], we found that mithramycin A, an antineoplastic antibiotic, markedly decreased SETDB1 expression and H3K9me3 in different cells. Mithramycin A subsequently led to reduced AKT methylation and phosphorylation (Fig. 7f; Supplementary Fig. 7b) and decreased the interaction between AKT1 and PDK1 (Fig. 7g). Biologically, mithramycin A attenuated the phosphorylation and colony formation of cells expressing AKT1-WT, but not in *AKT1/2*-depleted DLD1 cells or *AKT1*$^{K140/142R}$-edited HEK293 cells (Fig. 7h–j; Supplementary Fig. 7c–e). To explore the potential antitumour roles of mithramycin A in vivo, we treated nude mice bearing A375 or DLD1 xenografted tumours, and found that mithramycin A significantly decreased tumour growth compared with the vehicle treatment (Fig. 7k–n; Supplementary Fig. 7f–i). Conceivably, the reduction of SETDB1 expression mediated by mithramycin A decreased H3K9me3 and AKT phosphorylation (Supplementary Fig. 7j). Taken together, these results suggest that SETDB1 inhibition

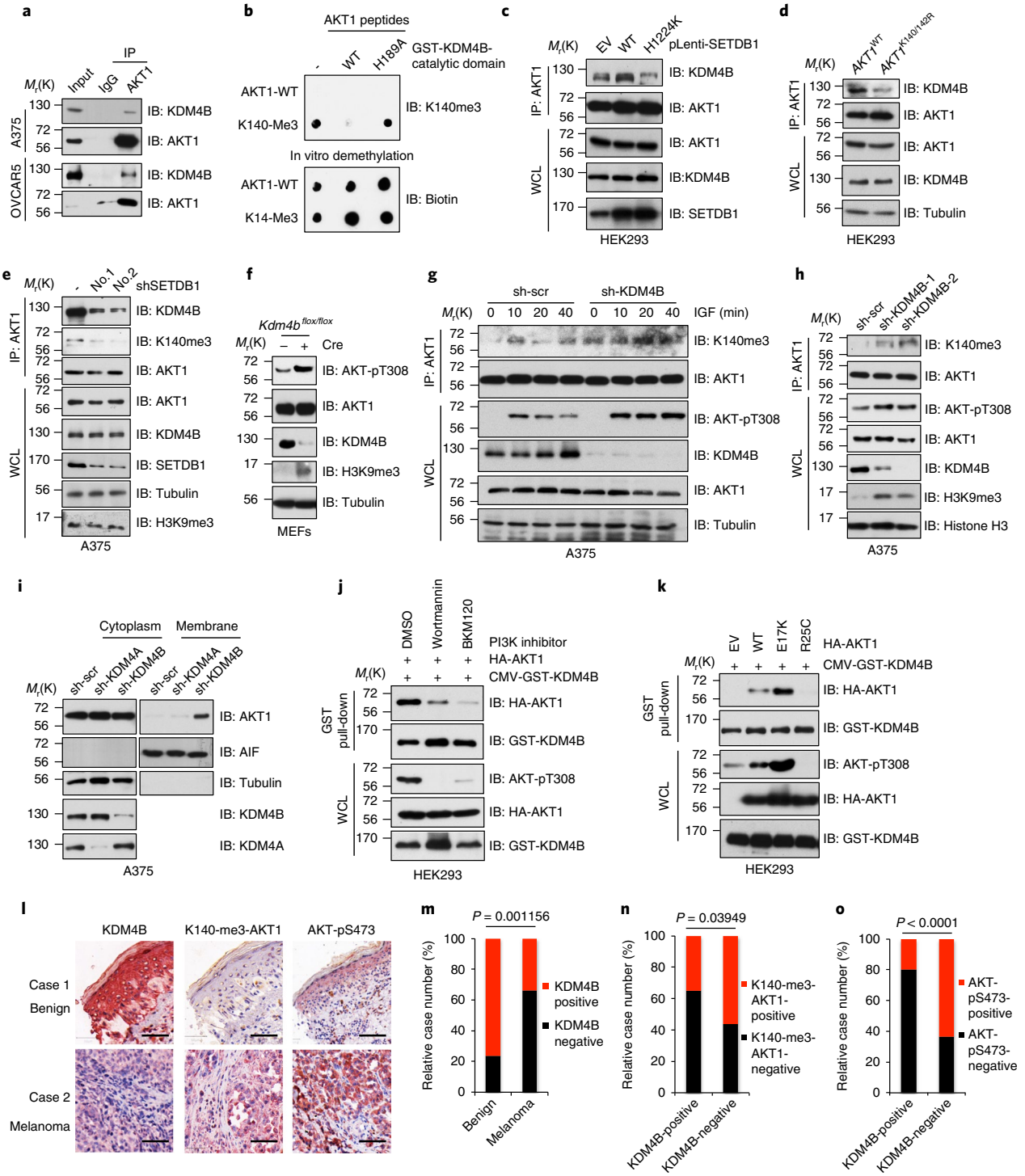

Fig. 6 | KMD4B demethylates AKT to inhibit AKT kinase activity. a,**c**–**e**, IB analysis of AKT1 IP products and WCL derived from A375 and OVACR5 cells (**a**), *SETDB1*-expressing HEK293 cells (**c**), *AKT1*$^{K140/142R}$-edited and parental HEK293 cells (**d**) and *SETDB1*-depleted A375 cells (**e**). IgG was used as a negative control. **b**, IB analysis of in vitro demethylation assays performed with synthetic AKT1-K140me3 peptides as substrate, and bacterially purified catalytic domain of KDM4B as the source of demethylase. **f**, IB analysis of WCL derived from primary *Kdm4b* conditional knockout MEFs infected with or without phage-Cre for 48 h before collection. **g**, A375 cells were lentivirally infected with shRNA against *KDM4B*. sh-scramble (sh-scr) was used as a negative control. Resulting cells were serum starved for 20 h, then stimulated with IGF (100 ng ml^{-1}) before collection for IP and IB analyses. **h**, IB analysis of IP products and WCL derived from A375 cells infected with lentivirus against *KDM4B*. **i**, IB analysis of cell fractionations separated from A375 cells lentivirally infected with shRNA against *KDM4B* or *KDM4A*. **j**,**k**, HEK293 cells were transfected with indicated constructs and treated with different PI3K inhibitors or dimethylsulfoxide (DMSO) for 1 h (**j**) before being subjected to GST pull-down assay and IB analyses. **l**–**o**, IHC staining of KDM4B, AKT1-pS473 and AKT1-K140me3 in a melanoma tissue microarray (**l**). Scale bar, 50 μm. The distribution of KDM4B staining is plotted in **m** ($n = 97$ tissue specimens). The correlations of AKT1-pS473 or AKT1-K140me3 with KDM4B are plotted in **n** ($n = 96$ tissue specimens; **o**, $n = 95$ tissue specimens). All *P* values were calculated using chi-squared tests. Detailed statistical tests are described in the Methods. Western blots were performed twice independently, with similar results obtained. Statistical source data for **m** and **n** are shown in Supplementary Table 2. Scanned images of unprocessed blots are shown in Supplementary Fig. 8.

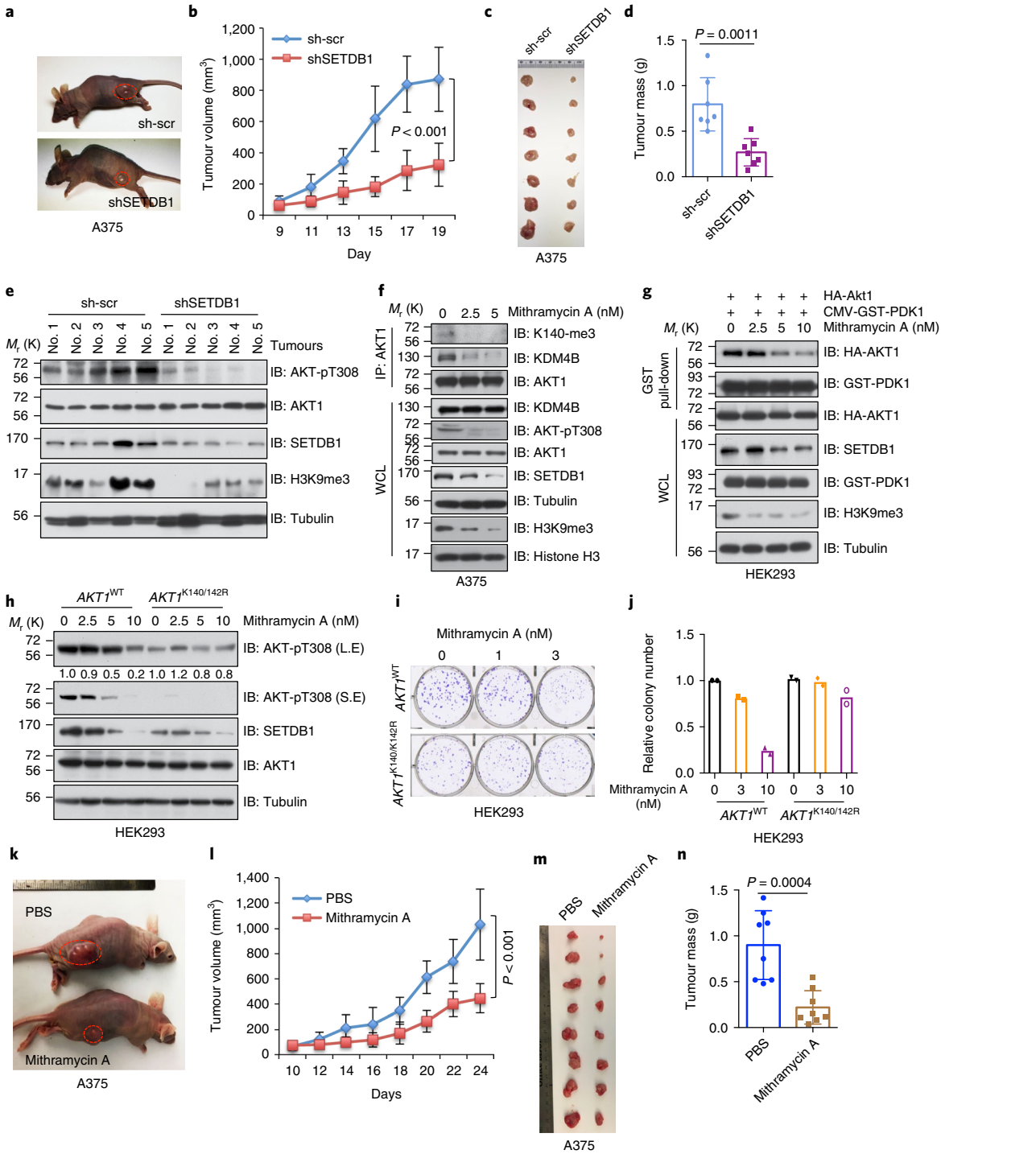

Fig. 7 | Deficiency of SETDB1 inhibits AKT kinase activity and oncogenic function. a–d, *SETDB1*-depleted A375 and control cells were subjected to mouse xenograft assays. Tumour sizes were monitored (**a**,**b**). Tumours were dissected (**c**) and tumour mass were weighed (**d**). Data represent the mean ± s.e.m., $n = 7$ mice. *P* values were calculated using two-way ANOVA (**b**) and two-tailed unpaired Student's *t*-test (**d**). **e**, The phosphorylation status of AKT1 (AKT-pT308) and methylation of H3K9 (H3K9me3) were detected by IB analysis with WCL derived from recovered xenografted tumours. **f**, IB analysis of IP products and WCL derived from A375 cells treated with different doses of mithramycin A for 72 h before collection. **g**, HEK293 cells were transfected with indicated constructs and treated with different doses of mithramycin A for 72 h before collection for GST pull-down assays and IB analysis. **h–j**, *AKT1*$^{K140/142R}$-edited and parental HEK293 cells were treated with different doses of mithramycin A for 72 h and subjected to IB analysis (**h**). The resulting cells were subjected to colony-formation (**i**) assay. The experiment was performed twice independently with three repeats, and exhibited similar results (**i**). Representative images are shown in **i** and relative colony numbers normalized with untreated cells derived from two independent experiments are plotted in **j**. **k–n**, Mithramycin A treatment reduced in vivo tumorigenesis of xenografted A375 cells. When the tumours of xenografted A375 cells reached 100 mm^3, the mice were treated with mithramycin A (0.2 mg per kg) or PBS (as a negative control). Tumour sizes were monitored (**k**,**l**) and tumour mass were weighed (**m**,**n**). Data represent the mean ± s.e.m., $n = 8$ mice. *P* values were calculated using two-way ANOVA (**l**) and two-tailed unpaired Student's *t*-tests (**n**). Detailed statistical tests are described in the Methods. Source data for **b**, **d**, **j**, **l** and **n** are shown in Supplementary Table 2. Scanned images of unprocessed blots are shown in Supplementary Fig. 8.

could benefit patients with cancer by repressing AKT oncogenic signalling in addition to its well-characterized role in reprogramming the epigenome (Supplementary Fig. 7k).

Discussion

To identify novel non-histone methylated proteins involved in oncogenic signalling pathways, we performed a MS-based high-throughput screen and detected numerous proteins modified by lysine trimethylation. We showed that AKT1 could be methylated in its linker region, which was enhanced during physiological conditions such as growth factor (insulin or IGF) stimuli or pathological conditions, such as the AKT1-E17K mutation or *PTEN* deficiency. Absence of AKT methylation repressed its kinase activity and markedly decreased cell growth, glucose uptake and tumorigenesis. More strikingly, methylation-deficient *Akt1* knock-in mice exhibited decreased body weight and size, which phenocopied *Akt1* knockout mice[46]. Importantly, we also observed that methylation-deficient *Akt1* knock-in could attenuate tumorigenesis in a carcinogen-induced skin tumour mouse model. Further investigations will be needed to determine whether knock-in methylation-deficient *Akt1* in genetic alteration models, such as $KRas^{G12D}$ mutation and *p53* depletion-mediated lung cancer models (*KP* mice)[47], could efficiently compromise lung tumorigenesis through decreased AKT activity.

Among the known upstream signals, AKT1-pT308 mediated by PDK1 is pivotal for AKT activation in a PtdIns(3,4,5)P_3-dependent fashion[48]. Here, we observed that SETDB1-mediated AKT methylation crosstalks with PI3K-mediated AKT phosphorylation. We suspect that the binding of PtdIns(3,4,5)P_3 to the PH domain of AKT could 'unlock' the AKT autoinhibition conformation. This conformation change could be necessary for SETDB1 to interact with the AKT PH domain and to methylate AKT in its exposed linker region, in turn enhancing the interaction of AKT with its upstream kinase PDK1 (Supplementary Fig. 5n). We also observed that SETDB1 enhanced the interaction of AKT with TRAF6 to facilitate AKT ubiquitination, subsequent PtdIns(3,4,5)P_3 binding and membrane translocation (Supplementary Fig. 5n). Our model suggests a loop of AKT activation triggered by PtdIns(3,4,5)P_3 accumulation or the AKT1-E17K mutation, which could be antagonized by the demethylase KDM4B (Supplementary Fig. 5n). Additionally, the SETDB1 Tudor domain interacts with AKT1 mainly in the context of the AKT1 linker region being methylated. Thus, we speculate that methylation of the linker region could be the primary modification that enhances the interaction of SETDB1 with AKT1, and sequentially promotes the methylation of AKT on other lysine residues (such as K64 in the PH domain of AKT). Consistent with our findings, another group also revealed that SETDB1-mediated AKT1 trimethylation at K64 plays an important role in AKT interacting with and being ubiquitinated by TRAF6 to facilitate AKT membrane translocation and kinase activation[49]. Therefore, the complicated connection and crosstalk of the SETDB1-mediated methylation of different lysine residues on AKT, including K140/K142 in the linker domain and K64 in the PH domain, warrants further investigation.

Finally, our study revealed that SETDB1 accelerates tumorigenesis largely through AKT activation in a methylation-dependent manner. As such, the function of SETDB1 is not restricted to the nucleus to repress gene transcription; SETDB1 also methylates non-histone proteins in the cytoplasm, such as AKT, to activate its oncogenic functions.

Online content

Any methods, additional references, Nature Research reporting summaries, source data, statements of data availability and associated accession codes are available at https://doi.org/10.1038/s41556-018-0261-6.

Received: 21 December 2017; Accepted: 10 December 2018;
Published online: 28 January 2019

References

1. Jones, P. A., Issa, J. P. & Baylin, S. Targeting the cancer epigenome for therapy. *Nat. Rev. Genet.* **17**, 630–641 (2016).
2. You, J. S. & Jones, P. A. Cancer genetics and epigenetics: two sides of the same coin? *Cancer Cell* **22**, 9–20 (2012).
3. Glaser, K. B. HDAC inhibitors: clinical update and mechanism-based potential. *Biochem. Pharmacol.* **74**, 659–671 (2007).
4. Fahy, J., Jeltsch, A. & Arimondo, P. B. DNA methyltransferase inhibitors in cancer: a chemical and therapeutic patent overview and selected clinical studies. *Expert Opin. Ther. Pat.* **22**, 1427–1442 (2012).
5. Delmore, J. E. et al. BET bromodomain inhibition as a therapeutic strategy to target c-Myc. *Cell* **146**, 904–917 (2011).
6. Kelly, T. K., De Carvalho, D. D. & Jones, P. A. Epigenetic modifications as therapeutic targets. *Nat. Biotechnol.* **28**, 1069–1078 (2010).
7. Daigle, S. R. et al. Potent inhibition of DOT1L as treatment of MLL-fusion leukemia. *Blood* **122**, 1017–1025 (2013).
8. Biggar, K. K. & Li, S. S. Non-histone protein methylation as a regulator of cellular signalling and function. *Nat. Rev. Mol. Cell Biol.* **16**, 5–17 (2015).
9. Chuikov, S. et al. Regulation of p53 activity through lysine methylation. *Nature* **432**, 353–360 (2004).
10. Guo, A. et al. Immunoaffinity enrichment and mass spectrometry analysis of protein methylation. *Mol. Cell. Proteomics* **13**, 372–387 (2014).
11. Saddic, L. A. et al. Methylation of the retinoblastoma tumor suppressor by SMYD2. *J. Biol. Chem.* **285**, 37733–37740 (2010).
12. Vanhaesebroeck, B. & Alessi, D. R. The PI3K–PDK1 connection: more than just a road to PKB. *Biochem. J.* **346**, 561–576 (2000).
13. Manning, B. D. & Toker, A. AKT/PKB signaling: navigating the network. *Cell* **169**, 381–405 (2017).
14. Ozes, O. N. et al. NF-kappaB activation by tumour necrosis factor requires the Akt serine-threonine kinase. *Nature* **401**, 82–85 (1999).
15. Yang, W. L. et al. The E3 ligase TRAF6 regulates Akt ubiquitination and activation. *Science* **325**, 1134–1138 (2009).
16. Liu, P. et al. Cell-cycle-regulated activation of Akt kinase by phosphorylation at its carboxyl terminus. *Nature* **508**, 541–545 (2014).
17. Guo, J. et al. pVHL suppresses kinase activity of Akt in a proline-hydroxylation-dependent manner. *Science* **353**, 929–932 (2016).
18. Mazur, P. K. et al. SMYD3 links lysine methylation of MAP3K2 to Ras-driven cancer. *Nature* **510**, 283–287 (2014).
19. Yoshioka, Y. et al. SMYD3-mediated lysine methylation in the PH domain is critical for activation of AKT1. *Oncotarget* **7**, 75023–75037 (2016).
20. Cong, L. et al. Multiplex genome engineering using CRISPR/Cas systems. *Science* **339**, 819–823 (2013).
21. Cho, H., Thorvaldsen, J. L., Chu, Q., Feng, F. & Birnbaum, M. J. Akt1/PKBalpha is required for normal growth but dispensable for maintenance of glucose homeostasis in mice. *J. Biol. Chem.* **276**, 38349–38352 (2001).
22. Nasti, T. H. et al. A murine model for the development of melanocytic nevi and their progression to melanoma. *Mol. Carcinog.* **55**, 646–658 (2016).
23. Gao, H. et al. Akt/PKB interacts with the histone H3 methyltransferase SETDB1 and coordinates to silence gene expression. *Mol. Cell. Biochem.* **305**, 35–44 (2007).
24. Liu, T. et al. Histone methyltransferase SETDB1 maintains survival of mouse spermatogonial stem/progenitor cells via PTEN/AKT/FOXO1 pathway. *Biochim. Biophys. Acta* **1860**, 1094–1102 (2017).
25. Cha, T. L. et al. Akt-mediated phosphorylation of EZH2 suppresses methylation of lysine 27 in histone H3. *Science* **310**, 306–310 (2005).
26. Cerami, E. et al. The cBio cancer genomics portal: an open platform for exploring multidimensional cancer genomics data. *Cancer Discov.* **2**, 401–404 (2012).
27. Schultz, D. C., Ayyanathan, K., Negorev, D., Maul, G. G. & Rauscher, F. J. 3rd SETDB1: a novel KAP-1-associated histone H3, lysine 9-specific methyltransferase that contributes to HP1-mediated silencing of euchromatic genes by KRAB zinc-finger proteins. *Genes Dev.* **16**, 919–932 (2002).
28. Ceol, C. J. et al. The histone methyltransferase SETDB1 is recurrently amplified in melanoma and accelerates its onset. *Nature* **471**, 513–517 (2011).
29. Macgregor, S. et al. Genome-wide association study identifies a new melanoma susceptibility locus at 1q21.3. *Nat. Genet.* **43**, 1114–1118 (2011).
30. Fei, Q. et al. Histone methyltransferase SETDB1 regulates liver cancer cell growth through methylation of p53. *Nat. Commun.* **6**, 8651 (2015).
31. Wong, C. M. et al. Up-regulation of histone methyltransferase SETDB1 by multiple mechanisms in hepatocellular carcinoma promotes cancer metastasis. *Hepatology* **63**, 474–487 (2016).
32. Carpten, J. D. et al. A transforming mutation in the pleckstrin homology domain of AKT1 in cancer. *Nature* **448**, 439–444 (2007).
33. Cao, J. et al. MC1R is a potent regulator of PTEN after UV exposure in melanocytes. *Mol. Cell* **51**, 409–422 (2013).
34. Dankort, D. et al. Braf(V600E) cooperates with Pten loss to induce metastatic melanoma. *Nat. Genet.* **41**, 544–552 (2009).

35. Garraway, L. A. et al. Integrative genomic analyses identify MITF as a lineage survival oncogene amplified in malignant melanoma. *Nature* **436**, 117–122 (2005).
36. Cantley, L. C. The phosphoinositide 3-kinase pathway. *Science* **296**, 1655–1657 (2002).
37. Alessi, D. R. et al. Characterization of a 3-phosphoinositide-dependent protein kinase which phosphorylates and activates protein kinase Balpha. *Curr. Biol.* **7**, 261–269 (1997).
38. Stephens, L. et al. Protein kinase B kinases that mediate phosphatidylinositol 3,4,5-trisphosphate-dependent activation of protein kinase B. *Science* **279**, 710–714 (1998).
39. Franke, T. F., Kaplan, D. R., Cantley, L. C. & Toker, A. Direct regulation of the Akt proto-oncogene product by phosphatidylinositol-3,4-bisphosphate. *Science* **275**, 665–668 (1997).
40. Chan, C. H. et al. The Skp2-SCF E3 ligase regulates Akt ubiquitination, glycolysis, herceptin sensitivity, and tumorigenesis. *Cell* **149**, 1098–1111 (2012).
41. Cederquist, C. T. et al. Systemic insulin sensitivity is regulated by GPS2 inhibition of AKT ubiquitination and activation in adipose tissue. *Mol. Metab.* **6**, 125–137 (2017).
42. Whetstine, J. R. et al. Reversal of histone lysine trimethylation by the JMJD2 family of histone demethylases. *Cell* **125**, 467–481 (2006).
43. Luo, J., Manning, B. D. & Cantley, L. C. Targeting the PI3K–Akt pathway in human cancer: rationale and promise. *Cancer Cell* **4**, 257–262 (2003).
44. Hennessy, B. T., Smith, D. L., Ram, P. T., Lu, Y. & Mills, G. B. Exploiting the PI3K/AKT pathway for cancer drug discovery. *Nat. Rev. Drug. Discov.* **4**, 988–1004 (2005).
45. Ryu, H. et al. *ESET*/*SETDB1* gene expression and histone H3 (K9) trimethylation in Huntington's disease. *Proc. Natl Acad. Sci. USA* **103**, 19176–19181 (2006).
46. Chen, W. S. et al. Growth retardation and increased apoptosis in mice with homozygous disruption of the *Akt1* gene. *Genes Dev.* **15**, 2203–2208 (2001).
47. DuPage, M., Dooley, A. L. & Jacks, T. Conditional mouse lung cancer models using adenoviral or lentiviral delivery of Cre recombinase. *Nat. Protoc.* **4**, 1064–1072 (2009).
48. Downward, J. Mechanisms and consequences of activation of protein kinase B/Akt. *Curr. Opin. Cell Biol.* **10**, 262–267 (1998).
49. Wang, G. H. et al. SETDB1-mediated methylation of Akt promotes its K63-linked ubiquitination and activation leading to tumorigenesis. *Nat. Cell Biol.* https://doi.org/10.1038/s41556-018-0266-1 (2019).

Acknowledgements

The authors thank B. North, J. Zhang, F. Dang and other Wei Lab members for critical reading of the manuscript, as well as members of the Pandofi and Toker Laboratory for helpful discussions. The authors thank H. Okada (Kindai University of Medicine) for the generation of *Kdm4b*$^{flox/flox}$ MEFs. W.G. is supported by K99CA207867 from the National Cancer Institute. W.W. is a LLS research scholar. This work was supported in part by the NIH grant CA177910 (to W.W. and A.T.). The MS work was partially supported by NIH grants P01CA120964 (to J.A.) and P30CA006516 (to J.A.)

Author contributions

J.G. designed and performed most of the experiments with assistance from X.D., B.L., W.G., P.L. W.W., P.P.P. and Y.S. A.T. supervised the study. J.G., N.Z. and J.Z. performed the revision. A.G. performed the IAP-LC-MS/MS screen. M.Y. and J.M.A. performed the MS work. J.G. and W.W. wrote the manuscript. All authors commented on the manuscript.

Competing interests

The authors declare no competing interests.

Additional information

Supplementary information is available for this paper at https://doi.org/10.1038/s41556-018-0261-6.

Reprints and permissions information is available at www.nature.com/reprints.

Correspondence and requests for materials should be addressed to W.W.

Publisher's note: Springer Nature remains neutral with regard to jurisdictional claims in published maps and institutional affiliations.

Methods

Cell culture, transfection and cell fractionations. Cell line sources are detailed in the Reporting Summary. All cell lines were free of mycoplasma contamination (tested by the vendor). HEK293, HEK293T, DLD1, OVCAR5 and A375 cells were cultured in DMEM medium supplemented with 10% fetal bovine serum (FBS), 100 units of penicillin and 100 μg ml^{-1} streptomycin. HCT116 *PTEN*$^{+/+}$ and *PTEN*$^{-/-}$ cells were gifts from T. Waldman (School of Medicine, Georgetown University). *Setdb1*$^{f/f}$*-ER-Cre* MEFs were gifts from Y. Shinakai and M. C. Lorincz[50]. DLD1-*AKT1/2*$^{-/-}$ and counterpart cells were provided by B. Vogelstein (Johns Hopkins University School of Medicine), and these cells were maintained in DMEM supplemented with 10% FBS. HIM cells were cultured in keratinocyte serum-free medium (Gibco Life Technologies), supplemented with epidermal growth factor (EGF; 5 ng ml^{-1}) and bovine pituitary extract (40 pg ml^{-1}). Cell transfection was performed using Lipofectamine and Plus reagents, as described previously[17]. Packaging of lentiviral shRNA- or complimentary DNA (cDNA)-expressing viruses and retroviral cDNA-expressing viruses, as well as subsequent infection of various cell lines, were performed according to previously described protocols[17]. Following viral infection, cells were maintained in the presence of hygromycin (200 μg ml^{-1}) or puromycin (1 μg ml^{-1}) depending on the viral vectors used to infect cells.

To prepare primary MEFs, *Jmjd2b*$^{flox/flox}$ mice were crossed, and fibroblasts were established from embryonic day 13.5 embryos according to standard procedures. In brief, the embryos were dissociated and then trypsinized to produce single-cell suspensions. The cells were maintained in DMEM supplemented with 10% fetal calf serum (FCS), L-glutamine and antibiotics. The cells were infected with phage-Cre lentiviruses for 2 days to delete *Jmjd2b*. *Kras;p53* and *Kras;p53;Smyd3*$^{-/-}$ cells derived from mouse lung and pancreas were obtained from P. K. Mazur (Stanford University School of Medicine)[18].

Cell fractionations were performed using a Cell Fractionation kit (Cell Signaling Technology, 9038). The kinase inhibitors wortmannin (Selleck, S2758), BKM120 (Selleck, S2247) and LY294002 (Selleck, S1105) were used at the indicated doses. Mithramycin A (Sigma, M6891), growth factors, including EGF (Sigma, E9644), insulin (Invitrogen, 41400-045) and IGF (Sigma, SRP3069), were used at the indicated doses. PtdIns(3,4,5)P_3 beads (P-B00Ss) and free PtdIns(3,4,5)P_3 (P-3908) were purchased from Echelon Biosciences.

Plasmid construction. Constructs of pcDNA3-HA-AKT1, pcDNA3-HA-AKT2, pcDNA3-HA-AKT3 and pcDNA3-HA-myr-AKT1, pcDNA3-HA-AKT1-E17K, pET-GSK3β and pCMV-Flag-PDK1 were produced as previously described[17]. pCMV-Flag-EZH2, pCMV-Flag-SET7, pCMV-Flag-SET8 and pCMV-Flag-MMSET were purchased from Addgene. pCDNA-Flag-SETDB1 and pCDNA-Flag-SETDB1-H1224K were gifts from G. P. Pfeifer[51]. pCMV-Flag-KDM4A, -KDM4B, -KDM4C and -KDM4D were obtained from Y. Shi (Harvard Medical School). pCMV-GST-PDK1, pCMV-GST-SETDB1, pCMV-GST-AKT1, pCMV-GST-AKT1-PH (aa1–108), pCMV-GST-AKT1-Linker (aa109–150), pCMV-GST-AKT1-KD (aa151–408), pCMV-GST-AKT1-HM (aa409–481), pCMV-GST-SETDB1-Tudor (aa257–318), pCMV-GST-KDM4A, pCMV-GST-KDM4C, pCMV-GST-KDM4D, pCMV-GST-KDM4B, pCMV-GST-KDM4B-jmj (aa1–180), pCMV-GST-KDM4B-Linker (aa181–425) and pCMV-GST-KDM4B-PHD-Tudor (aa181–425) were cloned into mammalian expression glutathione *S*-transferase (GST)-fusion vectors. Details of plasmid constructions are available upon request.

Various AKT1 and KDM4B mutants were generated using a QuikChange XL Site-Directed Mutagenesis kit (Stratagene) according to the manufacturer's instructions. All mutants were generated using mutagenesis PCR, and the sequences were verified by DNA sequencing. sh-*Akt1*-resistant mutants were generated with specific primers as previously described[16].

Antibodies. All antibodies were used at a 1:1,000 dilution in TBST buffer with 5% non-fat milk for western blotting. Anti-phospho-Ser473-AKT antibody (4060), anti-phospho-Thr308-AKT antibody (2965), anti-AKT1 antibody (2938), anti-AKT total antibody (4691), anti-PDK1 antibody (13037), anti-SMYD3 antibody (12859), anti-H3K9me3 antibody (13969), anti-pan-Kme3 antibody (14680), anti-AIF (apoptosis-inducing factor) antibody (5318), anti-histone H3 antibody (4499), anti-H3K4me2 antibody (9725), anti-phospho-Ser9-GSK3β antibody (5558), anti-GSK3β antibody (12456), anti-phospho-FOXO1 (Thr24)/FOXO3A (Thr32) antibody (9464), anti-FOXO3A antibody (2497), anti-GST antibody (2625), anti-pS6K1 (Thr389) antibody (9205), anti-S6K1 antibody (2708) and anti-pS240/244-S6 antibody (5364) were obtained from Cell Signaling Technology. Anti-SETDB1 antibody (11231) was obtained from Proteintech. Anti-KDM4A (A300-860A) and anti-KDM4B (A301-478A) antibodies were purchased from Bethyl. Anti-AKT1 agarose beads (sc-5298) and polyclonal anti-haemagglutinin (HA) antibody (sc-805) were obtained from Santa Cruz Biotechnology. Polyclonal anti-Flag antibody (F-2425), monoclonal anti-Flag antibody (F-3165, clone M2), anti-tubulin antibody (T-5168), anti-Flag agarose beads (A-2220), anti-HA agarose beads (A-2095), peroxidase-conjugated anti-mouse secondary antibody (A-4416) and peroxidase-conjugated anti-rabbit secondary antibody (A-4914) were obtained from Sigma. Monoclonal anti-HA antibody (MMS-101P) was obtained from Covance.

The polyclonal AKT1-K140me3 antibodies generated by Cell Signaling Technology were derived from rabbits, with each hydroxylation residue producing four clones. The antigen sequence used for immunization was AKT1 aa130–152 (GAEEMEVSLA**K**PKHRVTMNEFEY). **K** represents the trimethylation residue in this synthetic peptide. The antibodies were affinity purified using an antigen peptide column, but they were not counter-selected on unmodified antigen.

shRNAs, sgRNAs and CRISPR–Cas9-mediated knock-in and knockout assays. shRNAs against *SETDB1* were gifts from H. P. Koeffler[52], and shRNAs against *KDM4A* were gifts from C. Wang[53]. shRNAs against *KDM4B* were reported previously[20,54].

The lentiviruses for CRISPR–Cas9-based editing of *AKT1* were generated by cloning the annealed single guide RNAs (sgRNAs) into BsmBI-digested lentiCRISPR V2 vector, which encodes both Cas9 and an sgRNA of interest, as previously described[20]. The sgRNAs were designed using a CRISPR Design tool (crispr.mit.edu) and are as follows: sghAKT1 no.1 Forward: 5′-CACCGTGAAGAGATGGAGGTGTCCC-3′; Reverse: 5′-AAACGGGA CACCTCCATCTCTTCAG-3′; sghAKT1 no.2 Forward: 5′-CACCGTGGGGA CAGGCCTCACCACG-3′; Reverse: 5′-AAACCGTGGTGAGGCCT GTCCCCAC-3′.

For knock-in experiments, the lentiCRISPR V2 constructs containing sgRNA (as mentioned above) were co-transfected with template DNA into HEK293 cells. After selected with puromycin for 2 days, resulting cells were seeded into 96-well plates with 1 cell per well. After culture for ~2 weeks, the single clone was expanded to a 12-well plate, at the same time, the genomic DNA of each clone was collected using DNA Extract Solution (Epicentre), and PCR was performed with primers that covered the guide RNA sequence (~600 bp). The PCR products were digested with SacII, which can digest the knock-in genome but not the WT *AKT1* genome. The genomic DNAs of the digested clone were then subjected to sequencing to confirm the knock-in sequence. The examined clones were expanded and prepared for further studies.

The AKT-K140/142R guide DNA sequence is as follows: GGAGATGGACTTCCGGTCGGGCTCACCCAGTGACAACTCAGGGGC-TGAAGAGATGGAGGTGTCCCTCGCC**AGGCCGCGG**CATCGCGTGGTGAG-GCCTGTCCCCACTTCTGCCTGTGCCTGGGGCTGCCTTGGACTGTGGAGG GCTGGGTG (the bold text indicates mutant nucleotides that restore K140/142 to R140/142, and at the same time generate a new Sac II digest site. The underlined nucleotides indicate the destruction of the sgRNA recognition site).

Generation and validation of *Akt1*$^{K140/142R}$ knock-in mice. sgRNAs were synthesized using the in vitro transcription method (PNA Bio Company) with the following sequences: TGAAGAGATGGAGGTGTCCC and TGTGGTGAGTCTGGGCTCTG. Cas9 enzyme protein was obtained from PNA Bio. Mutated mouse genomic single strand template DNA (ssODN) was synthesized by Integrated DNA Technologies using the following sequence: GGA-CTCAAGAGGCAGGAAGAAGAGACGATGGACTTCCGATCAGGCTCACCC-AGTGACAACTCAGGGGCTGAAGAGATGGAGGTGTCCCTCGCC**AGGCCGC GG**CATCGTGTGGTGAGTCTGGGCTCTGCTTCTGCTGGGGCTGCCAGGGG TTGTGGAGGGACCTGGTAGGTCCTGGTATTCCTGCCTGGCTTCCTGTAT GG (the bold text indicates mutant nucleotides that restore K140/142 to R140/142, and at the same time generate a new Sac II digest site. The underlined nucleotides indicate the destruction of the sgRNA recognition site). The mixture of Cas9 protein (200 ng μl^{-1}), sgRNA(s) (100 ng μl^{-1}) and ssODN DNA (10–70 ng μl^{-1}) in 50 μl was utilized for generating knock-in mice by the transgenic facility at the Beth Israel Deaconess Medical Center.

The genomic DNAs derived from the tail of edited mice were extracted using QuickExtract DNA extraction solution (Epicentre, QE09050), and PCR was performed with the following primers: 5-AGGCCCAGGATCTGAGTGG (mAkt1-geno-5′) and 5-TCAGCGGGCATCTTCATATTAC (mAkt1-geno-3′). The PCR products were digested with Sac II for 1 h or subjected to Sanger sequencing with the primer 5-GACAAGCACTCTGCCAACTG (mAkt1-seq-3′). The validated heterogeneous knock-in mice (termed founder mice, P1) were selected and crossed to each other, and WT, heterogeneous and homogenous *Akt1*$^{K140/142R}$ knock-in mice were obtained (termed P2). Furthermore, we crossed homogenous knock-in mice with WT C57BL6 mice (Jackson Laboratories) and obtained the heterogeneous *Akt1*$^{K140/142R}$ knock-in mice (termed P3). Then we crossed these heterogeneous knock-in mice to each other and obtained WT, heterogeneous and homogenous knock-in mice (termed P4). At this time point, we monitored the body size, organ size as well as AKT signalling among WT, heterogeneous and homogenous *Akt1*$^{K140/142R}$ knock-in mice. To further diminish the nonspecific effect of genomic editing, we crossed back the homogenous knock-in mice (P4) with WT C57BL6 mice again to generate heterogeneous knock-in mice (P5) for further crossing and phenotype monitoring.

All experimental procedures were approved by the Institutional Animal Care and Use Committee (IACUC, RN150D) at the Beth Israel Deaconess Medical Center (protocol no. 043-2015). The research projects that are approved by the IACUC are operated according to the applicable institutional regulations. The Institute is committed to the highest ethical standards of care for animals used for the purpose of continued progress in the field of human cancer research.

IAP (Immunoaffinity purification)-LC–MS/MS screening. The experiments were performed as previously reported[10]. Briefly, OVCAR5 cell lysates were

proteolytically digested then purified over a Sep-Pak C18 cartridge. After dissolving in IAP buffer (50 mM MOPS, pH 7.2, 10 mM sodium phosphate, 50 mM NaCl), the recovered peptides were purified with trimethylation-specific antibodies. Finally, the enriched peptides were subjected to liquid chromatography (LC) tandem MS (LC–MS/MS) to identify the trimethylation sites in corresponding proteins.

Two-step chemical carcinogen-induced skin tumours. Two-step chemical carcinogen-induced skin tumours were generated as described previously[22]. In brief, the shaved naked back of 4–6-week-old WT or *Akt1*$^{K140/142R}$ knock-in mice were painted with 150 µg of DMBA (Sigma, D3254) dissolved in 200 µl acetone. After recovering for 2 weeks, the mice were treated with 20 µg of TPA (LC laboratories, P1680) in 200 µl acetone twice per week for 15 weeks. The neoplasms were monitored and then dissected out after the mice were killed. The samples were then subjected to haematoxylin and eosin (H&E) and IHC staining.

Immunoblot and immunoprecipitation analyses. Cells were lysed in EBC buffer (50 mM Tris (pH 7.5), 120 mM NaCl, 0.5% NP-40) supplemented with protease inhibitors (Complete Mini, Roche) and phosphatase inhibitors (phosphatase inhibitor cocktail set I and II, Calbiochem). The protein concentrations of whole cell lysates were measured using a Beckman Coulter DU-800 spectrophotometer and Bio-Rad protein assay reagent. Equal amounts of whole cell lysates were resolved by SDS–polyacrylamide gel electrophoresis (PAGE) and immunoblotted with indicated antibodies. For immunoprecipitation analysis, 1,000 µg lysates were incubated with the indicated antibody (1–2 µg) for 3–4 h at 4 °C followed by 1 h incubation with Protein A/G sepharose beads (GE Healthcare). The recovered immunocomplexes were washed five times with NETN buffer (20 mM Tris (pH 8.0), 150 mM NaCl, 1 mM EDTA and 0.5% NP-40) before being resolved by SDS–PAGE and immunoblotted with indicated antibodies. Quantification of immunoblot band intensities was performed using Image J software.

Melanoma and nevus tissue microarray and IHC staining. A tissue microarray containing 18 nevi, 33 metastatic melanomas and 49 malignant melanomas was obtained from Biomax (ME1004f).

IHC was performed on 4-µm-thick, formalin-fixed paraffin-embedded (FFPE) sections. FFPE sections were deparaffinized using xylene and rehydrated in graded ethanol. Sections were heated in a pressure cooker to 125 °C for 30 s and 90 °C for 10 s in citrate buffer (pH 6.0) for antigen retrieval. All sections were incubated with peroxidase (Dako, S2003) and protein blocking reagents (Dako, X0909) for 5 min each. Sections were then incubated with anti-AKT-pS473 (1:50; Cell Signaling Technology, 4060), anti-AKT-K140me3 (1:200), anti-pS420/424-S6 (1:1,500; Cell Signaling Technology, 5364) or anti-SETDB1 (1:100; Cell Signaling Technology, 93212) antibody diluted in Dako diluent with background-reducing components (Dako, S3022) for 1 h at room temperature. Following primary antibody incubation, sections were incubated with monoclonal mouse anti-rabbit immunoglobulins (Dako, M0737) for 30 min at room temperature. Afterwards, sections were incubated with Envision + System-HRP Labeled Polymer Anti-Rabbit (Dako, K4003) for 30 min. All sections were developed using a DAB chromogen kit (Dako, K3468) and lightly counterstained with haematoxylin. The score of the IHC signals was judged by two independent pathologists in a blinded manner.

Purification of GST- and His-tagged proteins from bacteria. Recombinant GST-conjugated KDM4B catalytic domain and histidine (His)-conjugated GSK3β were generated by transforming the BL21 (DE3) *Escherichia coli* strain with pGEX-KDM4B-Cata and pET-28a-GSK3β, respectively. Starter cultures (5 ml) grown overnight at 37 °C were inoculated (1%) into larger volumes (500 ml). Cultures were grown at 37 °C until an optical denisty of 0.8, following which protein expression was induced for 12–16 h using 0.1 mM IPTG (isopropyl-β-D-thiogalactoside) at 16 °C with vigorous shaking. Recombinant proteins were purified from collected pellets. Pellets were re-suspended in 5 ml EBC buffer and sonicated (5 cycles of 10 s each at 50% output). Insoluble proteins and cell debris were discarded following centrifugation in a table-top centrifuge (13,000 r.p.m. at 4 °C for 15 min). Each 1 ml of supernatant was incubated with 50 µl of 50% glutathione-sepharose slurry (Pierce) or Ni-beads (Qiagen) for 3 h at 4 °C. The glutathione beads were washed three times with PBS buffer (1 ml per wash) and stored at 4 °C in PBS buffer containing 10% glycerol or eluted by elution buffer. The Ni-beads were washed three times with 50 mM Tris-Cl (pH 8.0) containing 20 mM imidazole, and eluted by Tris buffers containing 100 mM imidazole. Recovery and yield of the desired proteins (or complexes) were confirmed by analysing 10 µl of beads by Coomassie blue staining and quantified against BSA standards.

Purification of His-AKT1 protein from insect S9 cells. *Akt1* cDNA was cloned into an insect cell expression vector, pFastBac-HT A (Invitrogen), in frame with a His tag at the amino terminus. Constructs were transformed into DH10Bac bacteria (Invitrogen) to generate bacmid DNAs. Akt baculoviruses were produced in Sf9 insect cells according to the manufacturer's specification. His-tagged proteins were purified on HisPur Cobalt resin (Thermo Scientific) and eluted using imidazole (Sigma). In brief, Sf9 insect cells expressing His-tagged Akt proteins were collected and washed once with ice-cold PBS. The cell pellet was then re-suspended for 30 min at 4 °C in lysis buffer containing 10 mM HEPES (pH 7.6), 3 mM $MgCl_2$, 300 mM KCl, 5% glycerol, 0.5% NP-40, 10 mM imidazole, 1 mM Na_2VO_4, 20 mM NaF, 1 mM sodium pyrophosphate, 25 mM β-glycerophosphate and complete EDTA-free protease inhibitors (Roche). The cell lysate was cleared by centrifugation for 20 min at 21,000 × *g* and 4 °C. While centrifuging the supernatant a second time in the same condition, HisPur Cobalt resin (Thermo Scientific) was equilibrated in the lysis buffer. The cell lysate was incubated with the resin for at least 1 h and afterward extensively washed with the lysis buffer. His-tagged Akt proteins were then eluted from the resin in several fractions using a buffer containing 10 mM HEPES (pH 7.6), 3 mM $MgCl_2$, 300 mM KCl, 10% glycerol and 250 mM imidazole.

Peptide synthesis and dot blot assays. Amino-terminal biotinylated peptides used for dot blot assays were synthesized at Tufts Medical School at 0.1 mmol scale. The sequences are as follows:

AKT1-K140-WT (aa131–151): AEEMEVSLAKPKHRVTMNEFE;
AKT1-K140me3: AEEMEVSLA*KPKHRVTMNEFE;
AKT1-K140/142me3: AEEMEVSLA*KP*KHRVTMNEFE (where the asterisk denotes trimethylation).

Peptides were diluted to 1 µM for further biochemical assays. For dot blot assays, peptides were spotted onto a nitrocellulose membrane, allowing the solution to penetrate (usually 3–4 mm diameter) by applying it slowly as a volume of 1 µl. The membrane was dried, and nonspecific sites were blocked by soaking in TBST buffer with 5% non-fat milk for immunoblot analysis as described previously[17].

AKT in vitro kinase assays. AKT in vitro kinase assays were performed using an adapted version of a previously described protocol[16]. Briefly, 1 µg of the bacterially purified His-GSK3β fusion proteins were incubated with immunoprecipitated AKT1 from HEK293 cells transfected with various mutant AKT1 in the presence of 100 ng [γS]ATP (Abcam, 138911) in kinase reaction buffer (50 mM Tris (pH 7.5), 1 µM $MnCl_2$, 2 mM dithiothreitol (DTT)) for 30 min at 30 °C. The reaction was subsequently stopped by adding in 0.1 mM EDTA, and further reacted for another 1 h by adding pNitrobenzyl mesylate (Abam, 138910) to alkylate the thiophosphorylation site on the substrates. The reaction was stopped by adding 3× SDS loading buffer and resolved by SDS–PAGE. Phosphorylation of His-GSK3β was detected by a specific antibody that recognizes the thiophosphate ester, as previously reported[55].

In vitro methylation and demethylation assays. The in vitro methylation assays were performed as previously described[56]. In brief, Flag-tagged SETDB1 was expressed and purified from HEK293T cells serving as the source of methyltransferase. The AKT1 proteins, including GST-tagged AKT1 expressed and purified from HEK293T cells, recombinant His-AKT1 obtained from ThermoFisher Scientific, or the AKT1 peptides synthesized from Tufts, were used as substrates. The reactions were performed in a solution of 50 mM Tris-HCl (pH 8.5), 5 mM $MgCl_2$, 4 mM DTT and 10 µM SAM at 37 °C for 6 h.

Demethylation assays were performed as reported previously[57]. In brief, the bacterially purified KDM4B catalytic domain (aa1–400) was used as the source of demethylase, and the synthetic AKT1-K140me3 peptides were used as the substrates. The reactions were performed in the a solution of 50 mM Tris-HCl (pH 8.2), 2% glycerol, 0.1% $MgCl_2$, 0.1% KCl and 0.1 mM phenylmethyl sulfonyl fluoride at 37 °C for 12 h.

In vivo ubiquitination assays. AKT ubiquitination assays were performed as reported previously[41]. Briefly, His-ubiquitin along with different variants of AKT1 were transfected into cells, and resulting cells were lysed in buffer A (6 M guanidine-HCl, 0.1 M Na_2HPO4/NaH_2PO_4 and 10 mM imidazole (pH 8.0)) and subjected to sonication. After high-speed centrifugation, the supernatants were incubated with nickel-beads (Ni-NTA; Qiagen) for 3 h at room temperature. The products were washed twice with buffer A, twice with buffer A/TI (1 volume buffer A and 3 volumes buffer TI), and one time with buffer TI (25 mM Tris-HCl and 20 mM imidazole (pH 6.8)). The pull-down proteins were resolved in 8% SDS–PAGE for immunoblot analysis.

MS analyses. For MS analyses, anti-HA immunoprecipitations were performed with the whole-cell lysates derived from three 10-cm dishes of HEK293 cells co-transfected with Flag-SETDB1 and HA-AKT1. The immunoprecipitated proteins were resolved by SDS–PAGE and identified by Coomassie staining. The band containing AKT1 was reduced with 10 mM DTT for 30 min, alkylated with 55 mM iodoacetamide for 45 min, and in-gel digested with trypsin enzymes. The resulting peptides were extracted from the gel and analysed by microcapillary reversed-phase (C_{18}) LC–MS/MS using a high-resolution QExactive HF Orbitrap (ThermoFisher Scientific) in positive ion data-dependent acquisition mode (Top 8) via higher energy collisional dissociation coupled to a Proxeon EASY-nLc II nano-HPLC[58]. MS/MS data were searched against the UniProt Human protein database (v.20151209, containing 21,024 entries) using Mascot 2.5.1 (Matrix Science), and data analysis was performed using Scaffold 4.4.8 software (Proteome Software).

Peptides and modified peptides were accepted if they passed a 1% false-discovery rate threshold.

Colony-formation assays. Cells were seeded into 6-well plates (300 or 600 cells per well) and left for 8–12 days until the formation of visible colonies. Colonies were washed with PBS and fixed with 10% acetic acid/10% methanol for 20 min, then stained with 0.4% crystal violet in 20% ethanol for 20 min. After staining, the plates were washed and air-dried, and colony numbers were counted.

Soft agar assays. Anchorage-independent cell growth assays were performed as described previously[16]. Briefly, the assays were performed using 6-well plates in which the solid medium consisted of two layers. The bottom layer contained 0.8% noble agar and the top layer contained 0.4% agar suspended with 1×10^4 or 3×10^4 cells. Complete DMEM (500 µl) was added every 7 days to keep the top layer moist, and 4 weeks later, the cells were stained with iodonitrotetrazolium chloride (1 mg ml^{-1}; Sigma, I10406) for colony visualization and counting.

Glucose uptake and lactate production assays. For glucose uptake assays, cells were cultured in 60-cm plates and were starved for 24 h with serum-free and glucose-free DMEM, then subjected to 20 µM 2-NBDG (Sigma, 72987) containing glucose-free DMEM for different time points. The cellular glucose uptake was quantified by fluorescence-activated cell sorting (FACS) analysis using BD FACSDiva 6.1.3 software.

For lactate production assays, cells were plated onto 60-cm plates and cultured for 24 h. Then the culture medium was collected, and lactate concentration was measured with lactate test strips and an Accutrend Lactate analyzer (Accutrend Lactate, Nova Biomedical). At the same time, viable cell numbers were counted under a microscope. The relative lactate production was calculated using the following formula: relative lactate production = lactate concentration/cell numbers. Date were normalized to the ratio obtained using control cells.

Mouse xenograft assays. Mouse xenograft assays were performed as described previously[4]. Briefly, 2×10^6 DLD1-*AKT1/2*$^{-/-}$ cells stably expressing WT or the K140/142R mutant form of AKT1, or 1×10^6 A375 cells with *SETDB1* knocked down, were injected into the flank of 8 female nude mice (NCRNU-M-M from Taconic, 4–5 weeks of age). Tumour size was measured every 3 days with a caliper, and the tumour volume was determined using the following formula: $L\times W^2\times0.5$, where L is the longest diameter and W is the shortest diameter. In the drug treatment group, when the tumour reached 100 mm^3, the mice were intraperitoneally injected with mithramycin A (0.2 mg per kg) or PBS (as a negative control) every other day. After ~18 days, mice were killed and the xenografted solid tumours were dissected. The tumour weights were measured and recorded post-necropsy.

Statistics and reproducibility. Statistical analyses (two-tailed Student's *t*-test) were performed using Prism 8 (GraphPad Software) for Figs. 1h, 2b,c and 7n, and Supplementary Fig. 7i in this manuscript. To calculate the *P* values between groups in Figs. 1f,j, 2h,l and 7b,l, and Supplementary Fig. 7g, two-way analysis of variance (ANOVA) was performed using Prism 8. Chi-squared tests were also performed to analyse the *P* values for Figs. 3j,l,m and 6m–o using Prism 8. All the calculated *P* values are indicated in the corresponding figures, and derived from three independent experiments with three technical replicates for each experiment. MS screens were performed twice successfully. All the western blots were performed twice independently, and similar results were obtained. In vitro methylation assays were performed once in Fig. 3e, and performed twice in Fig. 3g and Supplementary Fig. 3h independently, with similar results obtained. In vitro demethylation, ubiquitination, soft agar, colony formation, glucose uptake and lactate production assays were performed twice independently, with similar results obtained. To knockout or knockdown genes of interest, at least two independent sgRNAs or shRNAs were employed to generate cell lines, and similar results were found in all cell lines.

Reporting Summary. Further information on research design is available in the Nature Research Reporting Summary linked to this article.

Data availability

The MS-based screening data generated in this study have been deposited in ProteomeXchange under the accession code PXD011657. The SETDB1, EZH2, PTEN, EGFR, PIK3CA and AKT1 genetic alterations in TCGA datasets were integrated from the cBioPortal database (www.cbioportal.org), with the query of genes "ESET", "EZH2", "PTEN", "EGFR", "PIK3CA" and "AKT1" for both mutation and copy number alterations (CNAs) in different cancer types, such as BRCA and melanoma. Information regarding each cancer study is as follows: one dataset for BRCA (TCGA, provisional); one dataset for melanoma (TCGA, provisional). The source data for Figs. 1e,f,h,j–m, 2b,c,g,h, 3n,p,q, 4c,f,h,j,l,n, 6m–o and 7b,d,j,l,n, and Supplementary Figs. 1l,m, 2e,f, 3o, 4c–f,h and 7e,g,i have been provided as Supplementary Table 2. All other data supporting the findings of this study are available from the corresponding author upon reasonable request.

References

50. Liu, S. et al. Setdb1 is required for germline development and silencing of H3K9me3-marked endogenous retroviruses in primordial germ cells. *Genes Dev.* **28**, 2041–2055 (2014).
51. Li, H. et al. The histone methyltransferase SETDB1 and the DNA methyltransferase DNMT3A interact directly and localize to promoters silenced in cancer cells. *J. Biol. Chem.* **281**, 19489–19500 (2006).
52. Sun, Q. Y. et al. SETDB1 accelerates tumourigenesis by regulating the WNT signalling pathway. *J. Pathol.* **235**, 559–570 (2015).
53. Ding, X. et al. Epigenetic activation of AP1 promotes squamous cell carcinoma metastasis. *Sci. Signal.* **6**, ra28 (2013).
54. Kawazu, M. et al. Histone demethylase JMJD2B functions as a co-factor of estrogen receptor in breast cancer proliferation and mammary gland development. *PLoS ONE* **6**, e17830 (2011).
55. Allen, J. J. et al. A semisynthetic epitope for kinase substrates. *Nat. Methods* **4**, 511–516 (2007).
56. Shi, X. et al. Modulation of p53 function by SET8-mediated methylation at lysine 382. *Mol. Cell* **27**, 636–646 (2007).
57. Huang, J. et al. p53 is regulated by the lysine demethylase LSD1. *Nature* **449**, 105–108 (2007).
58. Breitkopf, S. B., Yuan, M., Helenius, K. P., Lyssiotis, C. A. & Asara, J. M. Triomics analysis of imatinib-treated myeloma cells connects kinase inhibition to RNA processing and decreased lipid biosynthesis. *Anal. Chem.* **87**, 10995–11006 (2015).

nature research

Corresponding author(s): Wenyi Wei

Reporting Summary

Nature Research wishes to improve the reproducibility of the work that we publish. This form provides structure for consistency and transparency in reporting. For further information on Nature Research policies, see Authors & Referees and the Editorial Policy Checklist.

Statistical parameters

When statistical analyses are reported, confirm that the following items are present in the relevant location (e.g. figure legend, table legend, main text, or Methods section).

n/a	Confirmed	
☐	☒	The exact sample size (*n*) for each experimental group/condition, given as a discrete number and unit of measurement
☐	☒	An indication of whether measurements were taken from distinct samples or whether the same sample was measured repeatedly
☐	☒	The statistical test(s) used AND whether they are one- or two-sided *Only common tests should be described solely by name; describe more complex techniques in the Methods section.*
☐	☒	A description of all covariates tested
☐	☒	A description of any assumptions or corrections, such as tests of normality and adjustment for multiple comparisons
☐	☒	A full description of the statistics including central tendency (e.g. means) or other basic estimates (e.g. regression coefficient) AND variation (e.g. standard deviation) or associated estimates of uncertainty (e.g. confidence intervals)
☐	☒	For null hypothesis testing, the test statistic (e.g. *F*, *t*, *r*) with confidence intervals, effect sizes, degrees of freedom and *P* value noted *Give P values as exact values whenever suitable.*
☐	☒	For Bayesian analysis, information on the choice of priors and Markov chain Monte Carlo settings
☐	☒	For hierarchical and complex designs, identification of the appropriate level for tests and full reporting of outcomes
☐	☒	Estimates of effect sizes (e.g. Cohen's *d*, Pearson's *r*), indicating how they were calculated
☐	☒	Clearly defined error bars *State explicitly what error bars represent (e.g. SD, SE, CI)*

Our web collection on statistics for biologists may be useful.

Software and code

Policy information about availability of computer code

Data collection	Zen (Zeiss) software was used to collect image. FACSDiva (BD Bioscience) software was used to collect flow cytometry data.
Data analysis	We used the Image J software to quantify the protein bands intensity and used the GraphPad (PRISM 8) to generate the graph figures and statistic analyses. We used Mascot 2.5.1 and vScaffold 4.4.8 to analyze the mass spectrometry results. We used BD FACSDiva 6.1.3 software for Flow analysis.

For manuscripts utilizing custom algorithms or software that are central to the research but not yet described in published literature, software must be made available to editors/reviewers upon request. We strongly encourage code deposition in a community repository (e.g. GitHub). See the Nature Research guidelines for submitting code & software for further information.

Data

Policy information about availability of data

All manuscripts must include a data availability statement. This statement should provide the following information, where applicable:

- Accession codes, unique identifiers, or web links for publicly available datasets
- A list of figures that have associated raw data
- A description of any restrictions on data availability

Source data for Fig. 1a and Supplementary Fig. 1a have been provided as Supplementary Table 1. The mass spectrometry-based screening data generated in this

study have been deposited in ProteomeXchange under the accession code PXD011657 and are available to the public. All other data supporting the findings of this study are available from the corresponding author on reasonable request.

Field-specific reporting

Please select the best fit for your research. If you are not sure, read the appropriate sections before making your selection.

☒ Life sciences ☐ Behavioural & social sciences ☐ Ecological, evolutionary & environmental sciences

For a reference copy of the document with all sections, see nature.com/authors/policies/ReportingSummary-flat.pdf

Life sciences study design

All studies must disclose on these points even when the disclosure is negative.

Sample size	No sample size calculations were performed. Sample size was determined according to our experience as well as literature reporting in terms of specific experiment.
Data exclusions	No samples or animals were excluded from the analyses
Replication	Multiple independent repeats were included for related experiments. Each experiment was performed for at least twice to make sure similar results are reproducible. Animal-related experiments and mass spectrometry experiments have been done once.
Randomization	6-8 week female nude mice were chosen as xenograft hosts. 10 days female and male WT and AKT1-K140/142R-Knockin mice were chosen to monitor the body weight. 4 weeks female and male WT and AKT1-K140/142R-Knockin mice were chosen for carcinogen treatment. All these mice were randomly allocated into experimental groups.
Blinding	For cell-based experiments Western blotting, immunostaining and FACS, cell types were known when prepare the samples or start to treat cells at the beginning of experiments. Data measurement for cell number and colony formation and soft agar assays were blinded to different person who processed assay at the time. IHC staining analysis were performed and analyzed blindedly.

Reporting for specific materials, systems and methods

Materials & experimental systems

n/a	Involved in the study
☒	☐ Unique biological materials
☐	☒ Antibodies
☐	☒ Eukaryotic cell lines
☒	☐ Palaeontology
☐	☒ Animals and other organisms
☒	☐ Human research participants

Methods

n/a	Involved in the study
☒	☐ ChIP-seq
☐	☒ Flow cytometry
☒	☐ MRI-based neuroimaging

Antibodies

Antibodies used

All antibodies were used at a 1:1000 dilution in TBST buffer with 5% non-fat milk for western blot.

Anti-phospho-Ser473-Akt antibody (Cell Signaling Technology, 4060), anti-phospho-Thr308-Akt antibody (Cell Signaling Technology, 2965), anti-Akt1 antibody (Cell Signaling Technology, 2938), anti-Akt total antibody (Cell Signaling Technology, 4691), anti-phospho-Ser9-GSK3b antibody (Cell Signaling Technology, 5558), anti-GSK3b antibody (Cell Signaling Technology, 12456), anti-phospho-FOXO1 (Thr24)/FOXO3A (Thr32) antibody (Cell Signaling Technology, 9464), anti-FOXO3A antibody (Cell Signaling Technology, 2497), anti-GST antibody (Cell Signaling Technology, 2625), anti-pS6K1 (Thr389) antibody (Cell Signaling Technology, 9205), anti-S6K1 antibody (Cell Signaling Technology, 2708) and anti-pS240/244-S6 antibody (Cell Signaling Technology, 5364), Anti-SETDB1 antibody (Proteintech, 11231), Anti-KDM4A antibody (Bethyl, A300-860A), anti-KDM4B antibody (Bethyl, A301-478A), polyclonal anti-HA antibody (Santa Cruz, 805), Polyclonal anti-Flag antibody (Sigma, F-2425), monoclonal anti-Flag antibody (Sigma, F-3165, clone M2), anti-Tubulin antibody (Sigma, T-5168), anti-Flag agarose beads (Sigma, A-2220), anti-HA agarose beads (Sigma, A-2095), peroxidase-conjugated anti-mouse secondary antibody (Sigma, A-4416) and peroxidase-conjugated anti-rabbit secondary antibody (Sigma, A-4914), Monoclonal anti-HA antibody (Covance, MMS-101P) . The polyclonal Akt1-K140-me3 antibodies generated by Cell Signaling Technology (CTS) were derived from rabbit, with each hydroxylation residue produced four clones. The antigen sequence used for immunization was Akt1 aa130-152 (GAEEMEVSLAKPKHRVTMNEFEY). K stands for tri-methylation residue in this synthetic peptide. The antibodies were affinity

purified using the antigen peptide column, but they were not counter selected on unmodified antigen.

Validation

All antibodies used in our study have been validated and detailed information could be found on the website from manufactures as listed below. Some of them have also been validated by our experiments as shown in this manuscript using either over-express, knockout or knockdown strategies.
phospho-Ser473-Akt, https://www.cellsignal.com/products/primary-antibodies/phospho-akt-ser473-d9e-xp-rabbit-mab/4060

phospho-Thr308-Akt, https://www.cellsignal.com/products/primary-antibodies/phospho-akt-thr308-c31e5e-rabbit-mab/2965?site-search-type=Products&N=4294956287&Ntt=%282965%29%2C&fromPage=plp&_requestid=740425

Akt1 antibody, https://www.cellsignal.com/products/primary-antibodies/akt-pan-c67e7-rabbit-mab/4691?site-search-type=Products&N=4294956287&Ntt=%284691%29%2C&fromPage=plp&_requestid=740463

Akt total antibody, https://www.cellsignal.com/products/primary-antibodies/akt1-c73h10-rabbit-mab/2938?site-search-type=Products&N=4294956287&Ntt=%282938%29%2C&fromPage=plp&_requestid=740451

phospho-Ser9-GSK3b antibody, https://www.cellsignal.com/products/primary-antibodies/phospho-gsk-3b-ser9-d85e12-xp-rabbit-mab/5558?site-search-type=Products&N=4294956287&Ntt=%285558%29%2C&fromPage=plp&_requestid=740494

GSK3bantibody, https://www.cellsignal.com/products/primary-antibodies/gsk-3b-d5c5z-xp-rabbit-mab/12456?site-search-type=Products&N=4294956287&Ntt=%2812456%29&fromPage=plp&_requestid=740502

phospho-FOXO1 (Thr24)/FOXO3A (Thr32) antibody, https://www.cellsignal.com/products/primary-antibodies/phospho-foxo1-thr24-foxo3a-thr32-antibody/9464?site-search-type=Products&N=4294956287&Ntt=+%289464%29&fromPage=plp&_requestid=740513

FOXO3A antibody, https://www.cellsignal.com/products/primary-antibodies/foxo3a-75d8-rabbit-mab/2497?site-search-type=Products&N=4294956287&Ntt=%282497%29&fromPage=plp&_requestid=740526

GST antibody, https://www.cellsignal.com/products/primary-antibodies/gst-91g1-rabbit-mab/2625?site-search-type=Products&N=4294956287&Ntt=%282625&fromPage=plp&_requestid=740541

pS6K1 (Thr389) antibody, https://www.cellsignal.com/products/primary-antibodies/phospho-p70-s6-kinase-thr389-antibody/9205?site-search-type=Products&N=4294956287&Ntt=%289205%29&fromPage=plp&_requestid=740549

S6K1 antibody, https://www.cellsignal.com/products/primary-antibodies/p70-s6-kinase-49d7-rabbit-mab/2708?site-search-type=Products&N=4294956287&Ntt=%282708%29&fromPage=plp

pS240/244-S6 antibody, https://www.cellsignal.com/products/primary-antibodies/phospho-s6-ribosomal-protein-ser240-244-d68f8-xp-rabbit-mab/5364?site-search-type=Products&N=4294956287&Ntt=5364%29&fromPage=plp&_requestid=740580

SMYD3 antibody, https://www.cellsignal.com/products/primary-antibodies/smyd3-d2q4v-rabbit-mab/12859?site-search-type=Products&N=4294956287&Ntt=smyd3&fromPage=plp

H3K9me3 antibody, https://www.cellsignal.com/products/primary-antibodies/tri-methyl-histone-h3-lys9-d4w1u-rabbit-mab/13969?site-search-type=Products&N=4294956287&Ntt=h3k9me3+&fromPage=plp

Pan-Kme3 antibody (14680), https://www.cellsignal.com/products/primary-antibodies/tri-methyl-lysine-motif-tme-k-d1l1x-rabbit-mab/14680?_=1541688963603&Ntt=Tri-Methyl-lys&tahead=true

AIF antibody, https://www.cellsignal.com/products/primary-antibodies/aif-d39d2-xp-rabbit-mab/5318?site-search-type=Products&N=4294956287&Ntt=aif&fromPage=plp

Histone H3 antibody, https://www.cellsignal.com/products/primary-antibodies/histone-h3-d1h2-xp-rabbit-mab/4499?site-search-type=Products&N=4294956287&Ntt=histone+h3&fromPage=plp

PDK1 antibody, https://www.cellsignal.com/products/primary-antibodies/pdk1-d4q4d-rabbit-mab/13037?site-search-type=Products&N=4294956287&Ntt=pdk1&fromPage=plp

anti-SETDB1, https://www.cellsignal.com/products/primary-antibodies/eset-d4m8r-xp-rabbit-mab/93212

H3K4me2, https://www.cellsignal.com/products/primary-antibodies/di-methyl-histone-h3-lys4-c64g9-rabbit-mab/9725?_=1541689459579&Ntt=H3K4me2,&tahead=true

SETDB1 antibody (11231), https://www.ptglab.com/products/SETDB1-Antibody-11231-1-AP.htm

KDM4A, https://www.bethyl.com/product/A300-860A/JMJD2A+Antibody

KDM4B, https://www.bethyl.com/product/A301-478A?referrer=search

Akt1 agarose beads, https://www.scbt.com/scbt/product/akt1-antibody-b-1

polyclonal anti-HA antibody (sc-805), https://www.scbt.com/scbt/product/ha-probe-antibody-y-11?requestFrom=search

Polyclonal anti-Flag antibody (F-2425), https://www.sigmaaldrich.com/catalog/product/sigma/f7425?lang=en&region=US

monoclonal anti-Flag antibody (F-3165, clone M2), https://www.sigmaaldrich.com/catalog/product/sigma/f3165?lang=en&region=US

Tubulin antibody (T-5168), https://www.sigmaaldrich.com/catalog/product/sigma/t5168?lang=en&region=US

Flag agarose beads (A-2220), https://www.sigmaaldrich.com/catalog/product/sigma/a2220?lang=en&region=US

HA agarose beads (A-2095), https://www.sigmaaldrich.com/catalog/product/sigma/a2095?lang=en&region=US

peroxidase-conjugated anti-mouse secondary antibody (A-4416), https://www.sigmaaldrich.com/catalog/product/sigma/a4416?lang=en&region=US

peroxidase-conjugated anti-rabbit secondary antibody (A-4914), https://www.sigmaaldrich.com/catalog/product/sigma/a4914?lang=en&region=US

Monoclonal anti-HA antibody (MMS-101P), https://www.biolegend.com/en-us/products/purified-anti-ha-11-epitope-tag-antibody-11374

Eukaryotic cell lines

Policy information about cell lines

Cell line source(s)	HEK293, HEK293T, DLD1, OVCAR5, HIM and A375 cells were obtained from American Type Culture Collection (ATCC). HCT116 PTEN+/+ and PTEN-/- cells were obtained from Dr. Todd Waldman in School of Medicine, Georgetown University. Setdb1f/f-ER-Cre mouse embryonic fibroblasts (MEFs) were obtained as gifts from Drs. Yoich Shinakai and Matthew C. Lorincz. DLD1-AKT1-/-AKT2-/- (termed AKT1/2-/-) and counterpart cells were kindly provided by Dr. Bert Vogelstein (Johns Hopkins University School of Medicine). Jmjd2bflox/flox MEFs were generated by Dr. Hitoshi Okada (Kindai University of Medicine). Kras;p53 and Kras;p53;sMYD3-/- cells derived from mouse lung and pancreas were obtained from Pawel K. Mazur at Stanford University School of Medicine.
Authentication	Cell lines were not authenticated.
Mycoplasma contamination	All cell lines tested negative for mycoplasma contamination.
Commonly misidentified lines (See ICLAC register)	HEK-293T cells were used to for lentiviral and retroviral production.

Animals and other organisms

Policy information about studies involving animals; ARRIVE guidelines recommended for reporting animal research

Laboratory animals	NU/J nude female mice at 4-6 week old were purchased from Taconic mouse facility. For Tumor xenograft models, tumor cells were injected subcutaneously into both flanks of 6-8 week old female nude mice. All animal experiments were approved by All experimental procedures were approved by the Institutional Animal Care & Use Committee (IACUC, RN150D) at Beth Israel Deaconess Medical Center with protocol #043-2015. The research projects that are approved by the IACUC are operated according the applicable Institutional regulations. AKT1-K140/142R knockin mice were generated by BIDMC transgenic facility with C57BL6 mice (Jackson Lab). 10 days female and male WT and AKT1-K140/142R-Knockin mice were genotyped and chosen to monitor the body weight. 4 weeks female and male WT and AKT1-K140/142R-Knockin mice were chosen for carcinogen treatment. All these mice were randomly allocated into experimental groups.
Wild animals	No wild animals involved in this study.
Field-collected samples	This study didn't involve samples collected from field.

Flow Cytometry

Plots

Confirm that:

☒ The axis labels state the marker and fluorochrome used (e.g. CD4-FITC).

☒ The axis scales are clearly visible. Include numbers along axes only for bottom left plot of group (a 'group' is an analysis of identical markers).

☒ All plots are contour plots with outliers or pseudocolor plots.

☒ A numerical value for number of cells or percentage (with statistics) is provided.

Methodology

Sample preparation	Cells were cultured in 60 cm plates, and were starved for 24 hrs with serum-free and glucose-free DMEM, then subjected to 20 uM 2-NBDG (Sigma 72987) containing glucose-free DMEM for different time points. Last, the cellular glucose uptake was

	quantified by FACS analysis.
Instrument	Using BD FACSCanto II Flow instrument
Software	Using BD FACSDiva 6.1.3 software to collect data and analyze data.
Cell population abundance	At least 10000 cells were analyzed for each sample.
Gating strategy	Cell population gating (FSC-Area VS FSC-Height) was adopted to make sure doublet exclusion and only single cell was used for analysis. A figure exemplifying the gating strategy is provided in the Supplementary Table 2.

☒ Tick this box to confirm that a figure exemplifying the gating strategy is provided in the Supplementary Information.